Progress in Organic Coatings 192 (2024) 108534

Contents lists available at ScienceDirect

Progress in Organic Coatings

journal homepage: www.elsevier.com/locate/porgcoat

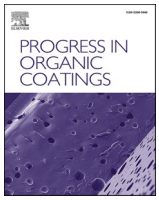

Post-service analysis of the degradation and protective mechanisms of chromate-based structural aircraft coatings

A.J. Cornet [a,b,*], A.M. Homborg [a,c], L. 't Hoen-Velterop [d], J.M.C. Mol [a]

[a] Delft University of Technology, Department of Materials Science and Engineering, Mekelweg 2, 2628CD Delft, the Netherlands
[b] Royal Netherlands Air Force, Kooiweg 40, 4631SZ Hoogerheide, the Netherlands
[c] Netherlands Defence Academy, Faculty of Military Sciences, P.O. Box 10000, 1780CA Den Helder, the Netherlands
[d] Royal Netherlands Aerospace Center, NLR, Voorsterweg 31, 8316PR Marknesse, the Netherlands

ARTICLE INFO

Keywords:
Thermo-oxidation
In-service coating degradation
Self-healing
Aluminium (hydr)oxide
Chromate-based structural aircraft coatings

ABSTRACT

The substitution of chromate-containing structural coating systems in aviation with alternatives complying with nowadays strict environmental, health and safety regulations remains a formidable challenge. This complexity is partly due to the absence of a standardized from-test-to-market methodology, including a performance comparison between chromate-containing and alternative coating systems. To address this gap, the present study delves into the identification of crucial degradation factors that merit inclusion in such a methodology. Concurrently, it investigates the protective mechanisms inherent in chromate-containing coating systems and proposes improvements that can be applied to alternative coating systems. This study entails a comprehensive post-service examination of the degradation of paint applied to an aircraft component with over 35 years of service, employing electrochemical, microscopic and spectroscopic techniques. The findings underscore the role of thermo-oxidation as a significant degradation factor in the aging process of such coatings. Furthermore, the investigation elucidates a notable phenomenon in which aluminium ions within the coating pores form an aluminium hydroxide gel onto which chromate adsorbs. This process contributes to an increase in pore resistance upon exposure to electrolyte, leading to a self-healing barrier effect within the coating. Remarkably, this self-healing mechanism continues to offer long-term protection even when the coating matrix is sub-optimally cured due to application errors. Furthermore, this study reveals that the significant changes in capacitance during immersion testing result primarily from inhibitor leaching, emphasizing the effectiveness of combining Electrochemical Impedance Spectroscopy (EIS) with Scanning Electron Microscopy (SEM) analysis for studying coating degradation.

1. Introduction

The aviation industry relies heavily on the use of aluminium alloy components due to their lightweight and high-strength properties [1]. However, relatively aggressive and varying atmospheric conditions, exposure to corrosive substances and the proximity of salt water environments may render these components susceptible to corrosion, which can compromise their structural integrity and overall performance [2]. To combat this issue, extensive research and development efforts have led to the implementation of extensive corrosion protective measures. One of the most effective methods employed to counter the effects of corrosion in the aviation industry is the application of a multilayered paint system [2,3]. The application of an organic coating typically involves a pretreatment, such as an anodized layer or a conversion coating, followed by the subsequent application of a primer layer for internal structural components. External surfaces usually require both a primer and a topcoat for optimal protection and durability [2,4,5].

To date, chromates have been used as the primary corrosion inhibitor type incorporated in these coating systems [6,7]. Despite its efficacy in active corrosion protection, chromates can be carcinogens, underscoring the need for safer alternatives [8]. Extensive scientific research has led to the development of alternative paint systems. These novel systems rely on sacrificial protection mechanisms, as seen in magnesium-rich primers [9], or on active corrosion protection technologies involving elements like lithium [10,11] or praseodymium [12]. Although these alternatives have found applications in external uses, the

* Corresponding author at: Delft University of Technology, Department of Materials Science and Engineering, Mekelweg 2, 2628CD Delft, the Netherlands.
E-mail address: A.J.Cornet@TUDelft.nl (A.J. Cornet).

https://doi.org/10.1016/j.porgcoat.2024.108534
Received 21 February 2024; Received in revised form 26 April 2024; Accepted 20 May 2024
Available online 23 May 2024

implementation of chromate-free solutions to safeguard structural components, remains challenging.

The complexity of structural components poses significant challenges in the adoption of alternative systems. The challenges arise from the nature of structural components, which are usually engineered to last for the life of the aircraft, which, sometimes exceeds 40 years [13]. Consequently, the selected coating system must exhibit at least similar long-term stability and durability. Furthermore, the lack of accessibility of these components for maintenance or reapplication of coatings once the aircraft is operational, underscores the crucial significance of an effective initial coating system.

Continuous scientific research and development of new paint systems for structural applications persists to enhance the performance and applicability of such coatings. However, simulating real-world aviation environments for testing purposes presents considerable challenges in this ongoing scientific endeavour [14,15]. The detailed evaluation of the impact of the in-service environment on the degradation of structural coatings remains a challenging research domain [16].

In the pursuit of a comprehensive understanding of structural coating degradation under in-service conditions, this study meticulously examined aged aircraft components. The investigation delved into the extent of degradation incurred in visual intact coatings on these components after being in service for more than 35 years. To elucidate the degradation in these coating systems, a multi-faceted scientific approach was employed, combining Electrochemical Impedance Spectroscopy (EIS) with Scanning Electron Microscopy (SEM) analysis and Attenuated Total Reflectance Fourier Transform Infrared Spectroscopy (ATR-FTIR).

EIS measurements were conducted to observe differences in electrochemical behaviour during an immersion test among various structural coatings on aircraft parts with different numbers of flight hours. These measurements were complemented with SEM analyses, where cross-sections of the coatings were analysed after varying immersion times in order to reveal the physical changes during immersion. This provided valuable background information about the obtained EIS measurement results. Energy Dispersive X-ray (EDX) analysis was utilized to clarify alterations in the elemental composition of the coating. Additionally, ATR-FTIR was employed to investigate whether the structural coatings had been affected by thermo-oxidation.

2. Materials and methods

2.1. Selection of aircraft component

Four distinct aircraft components were selected, each with different accumulated flight hours across their operational lifespan. An overview of this selection can be found in Table 1 and an image of the selected component type is shown in Fig. 1. This selection aimed to correlate potential variations in degradation patterns to different flight-hour accumulations. The details of these selection procedure, as well as the disassembly procedure and part configuration, have been documented in earlier work [17].

2.2. Sample description

This study focused on the degradation of structural coatings throughout their operational service life. Special attention was paid to the degradation of visually intact coatings after more than 35 years of service. Therefore, samples were extracted from the aluminium structure of the selected parts where the primer had remained visually intact. The study utilized a combination of SEM analysis and blueprint examination to elucidate the coating composition and substrate material. The aluminium structure and the derived samples were composed of aluminium alloy AA2024-T62. The applied coating system featured a chromic acid anodized layer, functioning as a pretreatment, with a thickness of approximately 2 μm (as per MIL-A-8625, Cl I), topped with an organic coating, which is a strontium chromate primer (conforming to MIL-PRF-23377) with a thickness of approximately 25 μm.

Table 1
Overview of the selected aircraft parts.

Part #	Flight hours (FH)	Year of manufacturing
#2547	2547	1984
#4215	4215	1983
#5183	5183	1983
#5903	5903	1985

2.3. Coating composition

The applied strontium chromate coating on aircraft components comprises various substances. Analysis of the Material Safety Data Sheet (MSDS) reveals that the coating contains strontium chromate, solvents and an epoxy resin combined with a curing agent. The epoxy resin is formulated using a diglycidyl ether of bisphenol-A (DGEBA), which, when combined with the curing agent triethylenetetramine (TETA), forms the binder matrix, as illustrated in Fig. 2. In this binder matrix, pigments such as strontium chromate are incorporated.

2.4. Analytical techniques

The first step in the analysis of coating degradation consisted of a detailed microscopic examination. Specifically, the SEM, Thermo Scientific™ Helios™ UXe DualBeam G4, equipped with an EDX detector and a Focus Ion Beam (FIB), was utilized. FIB-milling facilitated the creation of cross-sections of the coating. For imaging, an acceleration voltage of 5 kV was employed in both secondary electron (SE) mode and backscatter electron (BSE) mode. For EDX analysis, an acceleration voltage of 15 kV was used. Prior to the SEM analysis, all samples were coated with a carbon layer of approximately 20 nm to mitigate any potential charging effects.

Following the initial microscopic assessments, the study proceeded with long-term exposure experiments, exposing the samples to a 0.1 M NaCl solution. A section with a surface area of 20 cm^2 of each sample was intentionally exposed to the electrolyte, while the remainder of the sample was sealed off with sealant (PR-1440). Except for the new reference coating, these EIS measurements were performed on a 10 cm^2 surface area. At distinct intervals throughout the immersion period, electrochemical measurements were performed using EIS. Each EIS measurement was repeated six times to confirm reproducibility, using a Biologic VSP-300 potentiostat over a frequency range of 10^{-2}–10^5 Hz with 7 points per decade and a sinusoidal amplitude of 25 mV using a 2-electrode setup in a Faraday cage with the sample acting as working electrode and a carbon rod as the counter electrode. One selected EIS spectrum per coating type was fitted with equivalent circuits using ZView 4 from Scribner Associates Inc.

In addition, cross-sectional samples, prepared through FIB-milling, underwent detailed examinations employing SEM. These measurements were systematically conducted after varying immersion times to observe the degradation occurring during the EIS analysis. During these examinations, the samples underwent EDX analyses, ensuring a thorough assessment of the coating's structural integrity and elemental constituent composition.

For the acquisition of quantifiable data, the software ImageJ from FUJI was employed to analyse the SEM-EDX images. The initial step in this analysis involved the conversion of RGB-images into 32-bit binary images. Subsequently, the threshold function was applied to select a specific bandwidth in the grayscale image corresponding to the pigment under examination. Notably, in this investigative process, careful consideration was given to aligning the chosen bandwidth with the EDX results associated with the pigment of interest. This alignment ensured a meaningful interpretation of the changes observed in the coating during the immersion tests. This enabled the identification of a depletion front

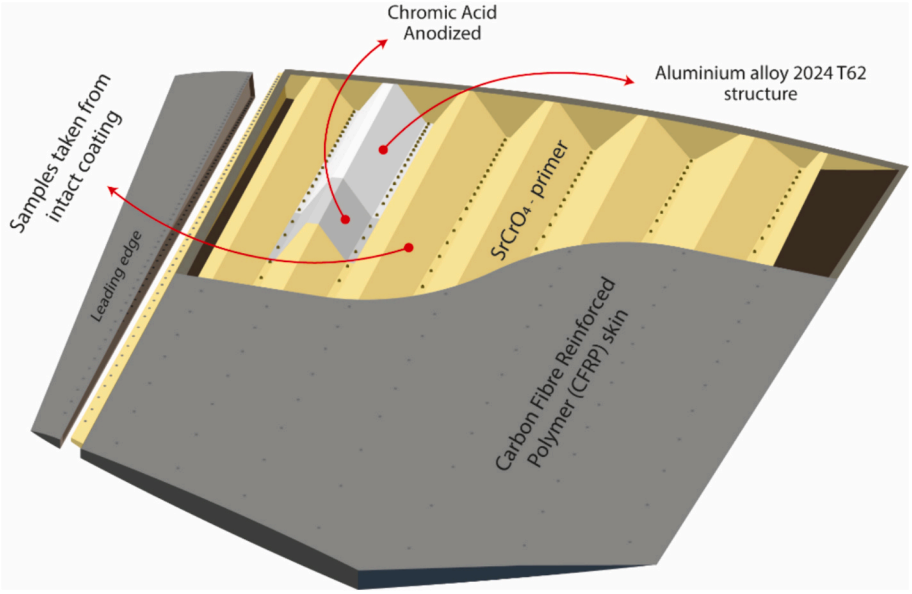

Fig. 1. Structural overview of selected aircraft part.

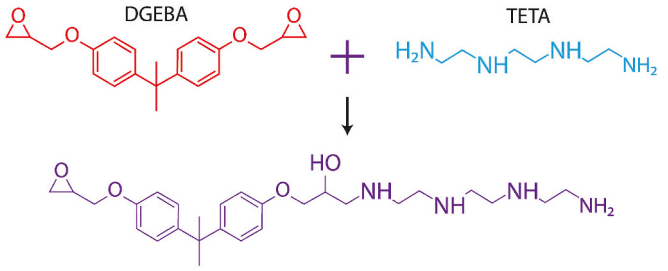

Fig. 2. Schematic representation of the epoxy matrix constituted by DGEBA resin and TETA hardener in the coating under investigation.

in coatings and allowed for the quantification of pigment leaching.

Further investigation was performed with ATR-FTIR analysis. This analytical technique, utilizing a Thermo Nicolet Nexus Fourier-Transform Infrared Spectrophotometer equipped with a mercury-cadmium-telluride (MCT) liquid-nitrogen-cooled detector and a Golden Gate sample holder, allowed for a profound examination of the polymer degradation within the coating. The spectroscopic measurements were taken at 4 cm^{-1} spectral resolution with 32 co-added scans.

To assess the impact of thermo-oxidation on the aircraft samples after service, ATR-FTIR spectroscopy analyses were conducted on these samples, without any prior exposure or additional aging. The data analysis of ATR-FTIR spectra utilized Spectragryph V1.2.16.1 software. Standardized processing procedures were applied to all spectra, commencing with advanced baseline correction, followed by chemometric preprocessing through standard normal variate (SNV) transformation. Subsequently, spectra within the 4000–1250 cm^{-1} range were normalized relative to the aromatic ring band of the epoxy matrix, specifically aligning with the ring stretching vibration at 1508 cm^{-1} [18]. In the 1350–650 cm^{-1} range, normalization was conducted at 840 cm^{-1}, corresponding to CH_3-bonds (C—H rocking) exclusive to the DGEBA structure [19]. These processing steps were required for inter-spectrum comparison.

2.5. Thermo-oxidation

To investigate the impact of thermo-oxidation on aircraft coatings during service, tests were conducted to identify the increase in surface temperature due to sunlight exposure under ambient conditions. The surface test panels, composed of CFRP material and coated with a matte grey military coating (Aerodur 5001), were positioned at a 45-degree angle. In this test setup, the surface test panels were placed on top of an aluminium box measuring approximately 120 × 60 × 5 cm. Two thermocouples were attached to the surface of the coated panel in order to measure the surface temperature during sunlight exposure. Additionally, two other thermocouples measured the temperature rise of the aluminium box, while ambient temperature was recorded using a fifth thermocouple. These tests were conducted in the Netherlands at the NLR facility in Marknesse from July to August 2021.

To further unravel the effects of thermo-oxidation in the investigated primer of the aircraft components, additional tests were performed on different samples exposed to various temperatures. The samples were coated with the same primer that was applied to the original aircraft components (MIL-PRF-23377) and contained a pretreatment consisting of a chromic acid-anodized substrate (MIL-A-8625). The samples were made of aluminium alloy AA2024-T62. After a post-painting curing period of 6 months under ambient laboratory conditions, these samples were exposed to different temperatures (75, 100, and 125 °C) for 7 days. Subsequently, ATR-FTIR measurements were conducted on the coatings to analyse the scission-effect in the polymer matrix during the various simulated thermo-oxidative exposures.

3. Results and discussion

3.1. General observations

The investigation of the coating commenced with a microscopic examination using SEM. Cross-sections of aircraft component samples, prepared through FIB milling as depicted in Fig. 3, unveiled the presence of diverse types of particles within the epoxy-polymer matrix. The subsequent EDX analysis, combined with data obtained from the primers MSDS, confirmed the presence of strontium chromate, talc, diatomaceous earth and titanium dioxide particles within the coating as identified in previous work [17]. It is noteworthy that the intact coating samples displayed an absence of discernible pores at the microscale, indicating minimal exposure to moisture. Consequently, the leaching of strontium chromate was deemed negligible, as discussed in our previous work [17].

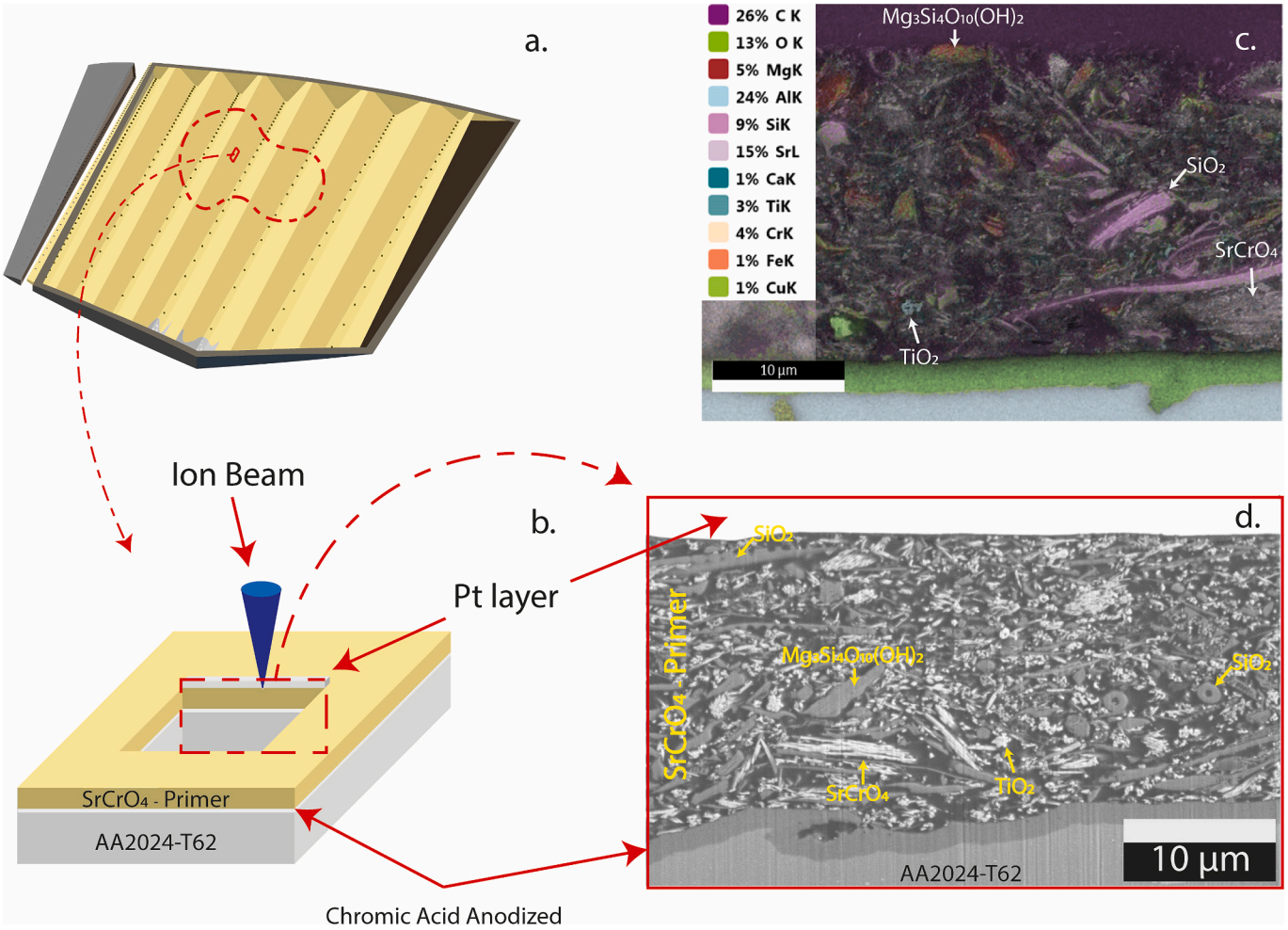

Fig. 3. Cross-sectional view of an intact coating achieved through FIB milling: (a) sample location within the overall aircraft part studied; (b) FIB-milling preparation method; (c) cross-sectional EDX mapping image; (d) cross-sectional BSE microscopic image [17].

3.2. Dissolution kinetics in epoxy coating

3.2.1. EIS measurement

Following the SEM analysis of the intact coating, samples of aircraft components underwent an immersion exposure in a 0.1 M NaCl solution. Subsequently, EIS measurements were performed, as illustrated in Fig. 4. The EIS Bode plots depict the recorded data after various immersion times (in hours) in 0.1 M NaCl solution for the aircraft coatings #2547, #4215, #5183, #5903 and a newly applied coating under laboratory conditions as a reference, in conjunction with SEM microscopy, conducted after various immersion times.

The following observations can be derived from the EIS measurements. Firstly, this analysis demonstrates a gradual decrease in impedance modulus value |Z| over immersion time for all coatings at low frequency (10^{-2} Hz). This behaviour indicates a decline in barrier properties [20]. Secondly, all coatings exhibited a decrease in |Z| over prolonged immersion time within the mid-frequency range (10^{0}–10^{3} Hz). This reduction signifies a concurrent increase in the coating's capacitance, as indicated by the phase angles ranging close to -90°, which suggests nearly a fully capacitive resistance [20–23]. This increase in capacitance is particularly pronounced for coating #2547, #4215 and #5903, and for the newly applied coating as well. By contrast, coating #5183 demonstrates distinctively different behaviour. It displays a 3 to 4 times smaller increase in capacitance than the other coatings. In addition to the increase in capacitance, another noteworthy observation can be made. When comparing the overall EIS spectra during immersion, it can be seen that the spectra of coatings #5903 and #4215 reach a stable final stage within 168 h, whereas coatings #2547, #5183 and the newly applied coating require longer immersion times and reach a stable stage only after 504 h.

The evaluation of coating degradation upon completion of the immersion test is quantifiable through EIS. An analysis of EIS data after 840 h of immersion reveals nuanced variations in coating performance on aircraft parts. This is specifically evident in the values of |Z| at both 10^{-2} Hz and 10^{2} Hz. The low-frequency values indicate the barrier properties, whereas the mid-frequency values illustrate the coatings' capacitive behaviour [20–23]. This approach allows the establishment of a performance hierarchy among the coatings, as depicted in Fig. 5. Remarkably, #5183 stands out as the best performer, exhibiting the highest barrier properties and the lowest capacitive behaviour. Coating #5183 is followed by #2547, the newly applied coating and #4215, which exhibit nearly equal performance. Coating #5903 performs slightly lower, which can be ascribed primarily to its lower capacitive behaviour.

Significantly, the sustained efficacy of all coatings, even after 840 h of immersion, is noteworthy. This is discernible through the consistent maintenance of effective protection, evidenced by the impedance modulus $|Z|_{0,01Hz}$ consistently exceeding 10^{8} Ω·cm^{2}. This underscores the enduring effectiveness in corrosion protection of each coating, providing valuable insights into their long-term performance and resilience under prolonged corrosive conditions [22,23].

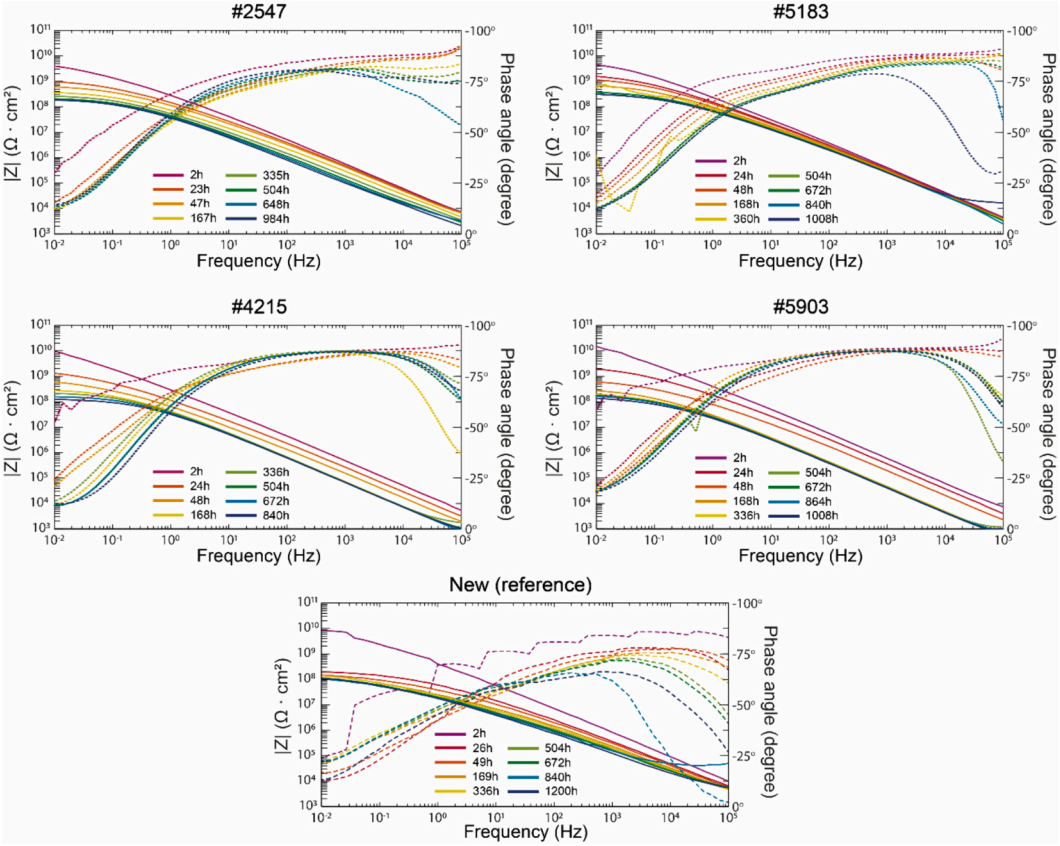

Fig. 4. EIS Bode plots recorded after various immersion times (in hours) in 0.1 M NaCl for coatings #2547, #4215, #5183, #5903 and a newly applied coating as a reference.

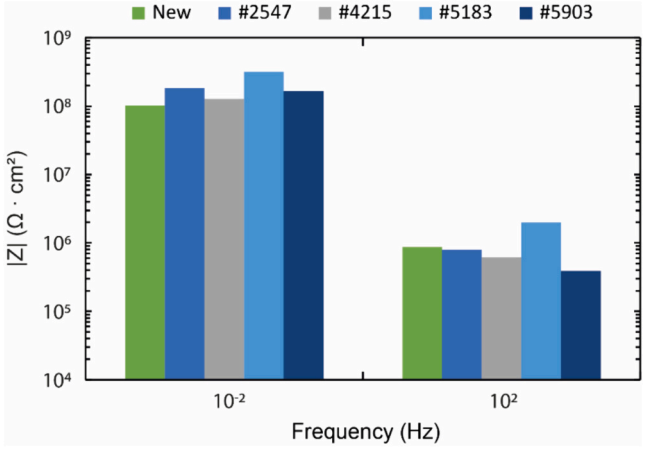

Fig. 5. |Z| at completion of the immersion test (840+ hours) in 0.1 M NaCl of the reference coating and coatings #2547, #4215, #5183 & #5903.

3.2.2. *Equivalent electrical circuit analysis*

The results of EIS spectra underwent fitting using an Equivalent Electrical Circuit (EEC), to precisely quantify the electrochemical characteristics of the coating and gain deeper insights into barrier properties, the capacitance behaviour and the diffusion processes at the interface. The selection of the EEC is performed with the use of the Bode plot diagrams presented in Fig. 4, which reveal the presence of two distinct time constants in the degrading coatings. These time constants manifest in both the low-frequency region (10^{-2}–10^{-1} Hz) as well as the mid-frequency region (10^{0}–10^{3} Hz) [24]. The specific EEC used for fitting is illustrated in Fig. 6e. It represents a circuit that contains two-time-constants, which is commonly employed to characterize a defective coating [21,24–26].

In this circuit, R_S refers to the electrolyte resistance [24–27]. The CPE_c indicates the Constant Phase Element (CPE), representing the non-ideal capacitance behaviour of the coating, while the R_C signifies the pore resistance of the organic coating [24–26]. The CPE_{dl} represents the non-ideal double-layer capacitance [24–26]. Together with the charge transfer resistance R_{ct}, these elements represent the electrochemical corrosion process at the coating-metal interface [24–26,28].

All fitting outcomes demonstrate an acceptable fit with a minimum chi-square of 2×10^{-3}, confirming the appropriateness of the chosen equivalent circuit for describing the electrochemical behaviour of the coatings [29,30].

In the fitting procedure, CPEs are used to accommodate the non-ideal capacitance behaviour of the coating and the electrochemical corrosion process at the coating-metal interface. To calculate the effective coating capacitance of a CPE at the corresponding time constant, the following Equation was used [31]:

$$C = \frac{(Q \bullet R)^{\frac{1}{n}}}{R} sin\left(\frac{n\pi}{2}\right) \quad (1)$$

The initial observation from the EEC fitting results reveals a noteworthy trend in the pore resistance of the coatings during immersion in 0,1 M NaCl. Initially a significant decrease is observed, followed by a gradual increase, as illustrated in Fig. 6a. The initial decrease, noted after 2 h of immersion, can be attributed to the rapid water uptake by the aged coatings. However, the subsequent increase in pore resistance after 48 h of immersion stands in contrast to what may have been expected - a decrease assumed to be solely due to the permeation of electrolyte in the coating and leaching of the strontium chromate inhibitor, resulting in an increased number of conductive pathways inside the coating [26,27].

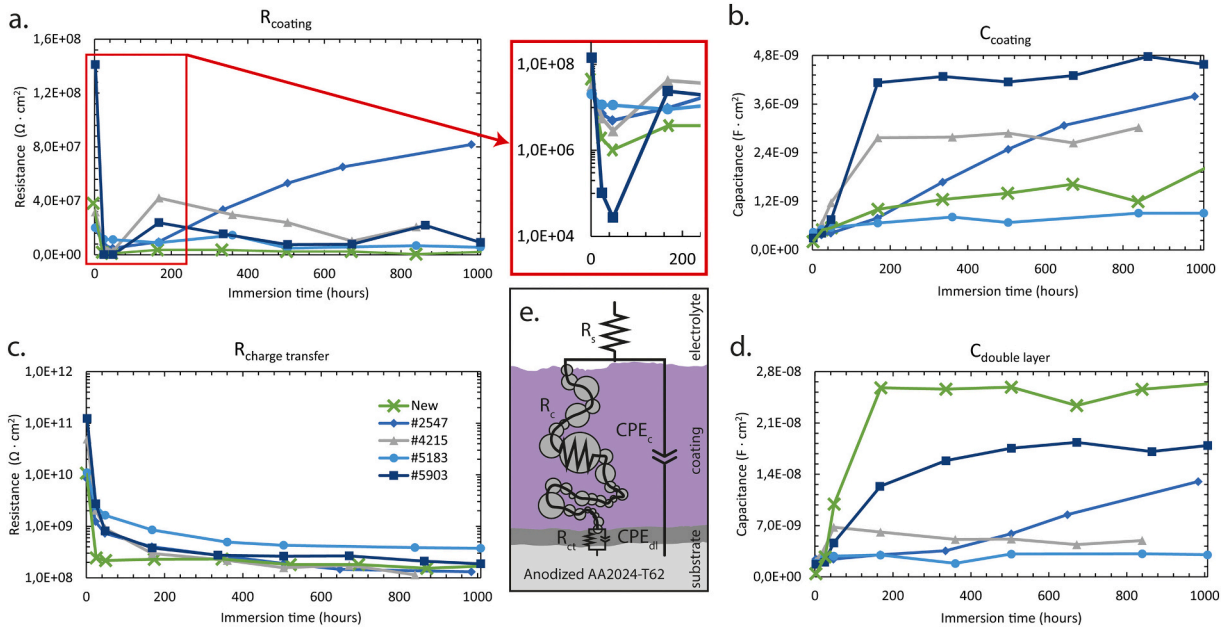

Fig. 6. Temporal evolution of fitted parameters during immersion tests. (a) Pore resistance R_c, (b) effective coating capacitance CPE_c, (c) charge transfer resistance R_{ct} and (d) effective double-layer capacitance CPE_{dl} and (e) corresponding equivalent electrical circuit.

However, the contrary is observed. This unexpected behaviour is also evident in the phase diagrams of the bode plots illustrated in Fig. 4, where a dip exists in the mid-frequency range between 10^0 Hz and 10^2 Hz until 48 h of immersion, after which the phase angle increases again. This behaviour is also reported in prior literature, where it is ascribed to the possible formation of corrosion product, which could increase the total resistance [32]. Notably, coating #5183 deviates from this pattern, exhibiting more expected behaviour including a rapid initial drop followed by stabilization of the resistance, which is indicative for electrolyte permeation inside the coating [21–23].

The capacitive behaviour of the coatings yielded intriguing results. Firstly, it was observed that coatings #5903 and #4215 exhibited a rapid and substantial increase in capacitance, whereas this increase was notably slower for coating #2547 and for the newly applied coating. This phenomenon can be attributed to the leaching rate of strontium chromate, which, in turn, augments the pores in the coating and consequently increases the capacitance [33,34]. The slower increase in capacitance for coating #2547 and for the newly applied coating can probably be attributed to a more intact polymer matrix, which limits the leaching rate of strontium chromate as compared to coatings that have been in service for an extended period of time [35]. However, coating #5183 did not display a substantial increase in capacitance, suggesting that leaching likely did not occur to a significant extent. The slight increase in capacitance in coating #5183 may be ascribed to water uptake by the coating, a process typically occurring within the first 24 h [33,36–39].

The authors suggest that the behaviour of the double-layer capacitance would follow a pattern similar to that of the coating capacitance. As the coating capacitance increases, a larger quantity of electrolyte can access the coating-metal interface. The electrolyte at this interface, initially in small quantities that increase over prolonged immersion, facilitates the electrochemical (corrosion) processes locally, resulting in sites where corrosion products developed at the coating-metal interface [34]. This corrosion product, fully saturated with electrolyte, induces a double-layer capacitance and a charge transfer resistance [34]. The charge transfer resistance indicates that the kinetically controlled electrochemical reactions at the interface behave as expected, consistently decreasing over immersion time [27,40,41]. This is primarily due to the increase in electrochemically active locations at the interface, collectively diminishing the total charge transfer resistance [34]. Consequently, this process leads to a simultaneous increase in double-layer capacitance [36,37].

While the behaviour of the double layer capacitance of all coatings aligned with the anticipated pattern, coating #4215 exhibited different characteristics. Initially demonstrating an increase, the double layer capacitance gradually diminished after 48 h of immersion. The authors currently lack an explanation for this unexpected behaviour, especially when contrasting this with the trend as observed in the charge transfer resistance. It would be expected that the double-layer capacitance of coating #4215 should follow the trend as observed with the coating capacitance, mirroring the behaviour of the other coatings.

Another observation that requires clarification is the significant increase in double layer capacitance observed for coating #2547 as well as for the new coating. This behaviour could be attributed to a more intact polymer matrix. In a more intact coating, the matrix protects strontium chromate particles within the coating from dissolving in the exposed electrolyte. Consequently, the electrolyte inside the coating contains less dissolved chromate, potentially leading to increased corrosion activity at the aluminium substrate. The authors suggest that this phenomenon is reflected in the increase in double layer capacitance as well as in the decrease in charge transfer resistance for coating #2547 and for the newly applied coating as reported in prior literature [42].

3.2.3. *SEM analysis of FIB-milled cross sections*

To gain a more comprehensive understanding of the processes occurring within the coating, SEM microscopy was employed to monitor the physical changes in the coating after various immersion times, as illustrated in Fig. 7. The depletion front, representing the extent of strontium chromate leaching due to immersion in a 0.1 M NaCl solution, is delineated by a red line in Fig. 7. Confirmation of strontium chromate dissolution is provided by the accompanying EDX analysis, substantiating the observations from the EIS analysis.

The extent to which the depletion front reaches the coating-metal interface varies among the different coatings and immersion times. For instance, coatings #4215 and #5903 exhibit the depletion front reaching the interface within 168 h. In contrast, for #2547 and #5183, the presented images in Fig. 7 indicate that the depletion front has not reached the interface even after 1008 h. It is essential to acknowledge

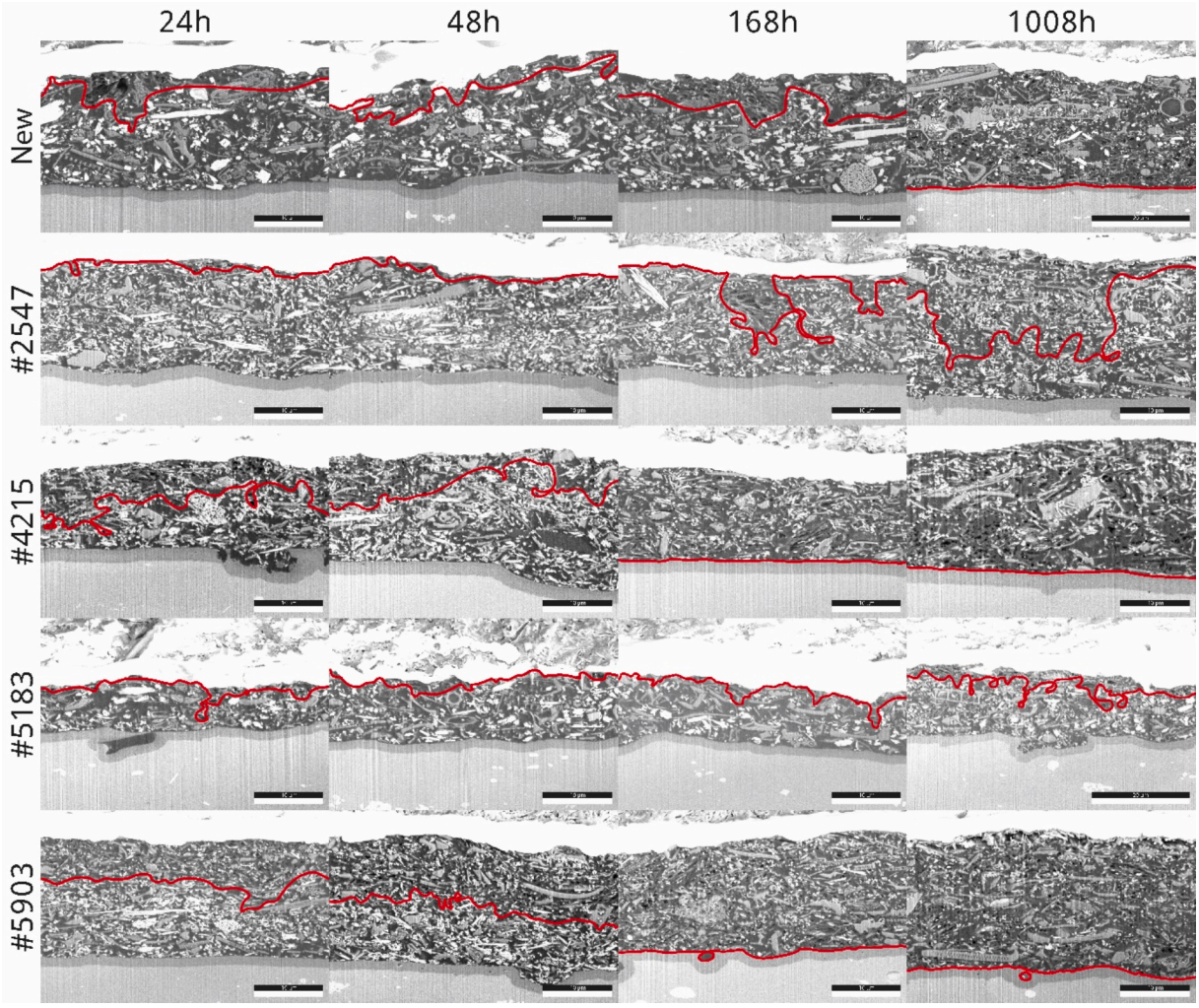

Fig. 7. SEM images of FIB-milled coated samples at varying immersion times, with the red line indicating the depletion front of strontium chromate particles for coatings #2547, #4215, #5183 and #5903. (For interpretation of the references to color in this figure legend, the reader is referred to the web version of this article.)

that the provided images are momentary and local and do not definitively rule out the chances of the depletion front reaching the interface at other locations for #2547 and #5183. From that perspective, EIS measurements offer more insight into the extent to which the leaching front has reached the coating-metal interface as it provides a more global view.

To quantitatively interpret the SEM-EDX findings, ImageJ was used to determine the percentage of strontium chromate. The leaching of strontium chromate was then plotted as a decrease in volume percentage of the coating and compared with the variation in coating capacitance

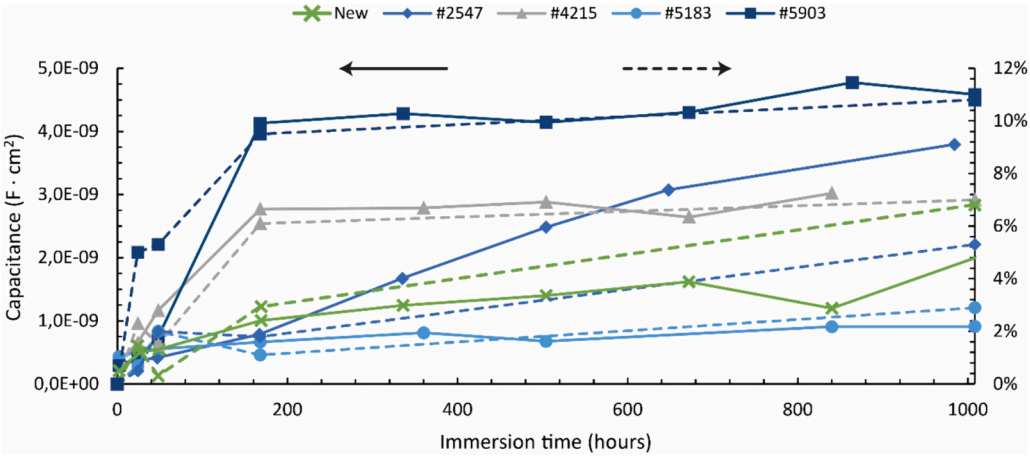

Fig. 8. Temporal evolution of coating capacitance (continuous lines) of aged aircraft components during immersion in 0.1 M NaCl, juxtaposed with the time-dependent release of strontium chromate (dashed lines).

over time, as illustrated in Fig. 8. This approach allows to utilize strontium chromate leaching during immersion to elucidate the fluctuations in coating capacitance. A striking observation is the consistent pattern: the leaching of strontium chromate corresponds well with the coating capacitance. This observation confirms that the increase in coating capacitance can be ascribed to strontium chromate leaching.

3.2.4. Pore resistance and aluminium mobility

It is remarkable that a coating with a significant number of pores shows $|Z|_{0.01Hz}$ values in the range of 10^8 Ω·cm^2. This phenomenon cannot be solely ascribed to the presence of an intact anodized layer, which typically offers $|Z|_{0.01Hz}$ values in the range of 10^6–10^7 Ω·cm^2 [43–45]. The implication is that the coating, despite its numerous pores, continues to provide robust resistance, a seemingly unconventional observation [46]. Consequently, the investigation into the development of pore resistance has become a subject of particular interest, warranting a more in-depth exploration.

Building upon the findings of Dong et al., where iron from the substrate is detected in the coating post-immersion in an electrolyte, the authors hypothesized that the diffusion of aluminium ions may potentially contribute to the increased pore resistance observed after 48 h of immersion in 0.1 M NaCl, as illustrated in Fig. 6 [47]. To test this hypothesis, SEM-EDX analysis was employed to scrutinize the presence of aluminium within FIB-milled cross-sections of the coating. This analysis was conducted on all coatings after various immersion times, with an illustrative example provided for coating #5903 in Fig. 9 after 48 h of immersion. Fig. 9 showcases a processed EDX map of the element aluminium superimposed on the SEM-BSE image. The contrast of the EDX map was adjusted using ImageJ in order to enhance the visibility of elemental aluminium within the coating.

This analysis suggests mobility of aluminium ions within the coating matrix. A notable difference of aluminium presence is apparent within the coating when comparing this below and above the depletion front respectively, as illustrated in Fig. 9c. The presence of aluminium below the depletion front is particularly visible around particles inside the coating, most notably in the proximity of silicon oxide and strontium chromate particles. The presence of aluminium around silicon oxide particles can be explained by the presence of talc, which contains silicon oxide and aluminium impurities which can replace silicon in the silica tetrahedral layer of the talc structure. [48–51]. However, the presence of aluminium around the strontium chromate particles remains unclear.

Further investigation of the aluminium distribution above the depletion front revealed the absence of aluminium within the pores resulting from the complete dissolution of strontium chromate. This phenomenon may be attributed to faster outward diffusion kinetics directed towards the electrolyte that is readily available in larger pores upon immersion. Conversely, slower diffusion is expected through smaller pores, potentially explaining the presence of aluminium below the depletion front within the coating. This intricate behaviour still necessitates further investigation for a comprehensive understanding.

In addition to confirming the presence of elemental aluminium in the coating, visual observations of samples after immersion in electrolyte highlights the development of a gel-like substance on top of coating #5184, as illustrated in Fig. 10. EDX analysis in the SEM suggests that the gel-like substance is primarily composed of aluminium (hydr)oxide, with minor traces of chromium, likely originating from chromate, and traces of NaCl. The results are presented in Table 2. It is crucial to emphasize that the aluminium detected in this gel product originates exclusively from the substrate beneath the exposed coating, given that all other regions of the substrate are effectively sealed with a protective sealant. This finding indicates that aluminium transport takes place through the coating during immersion in an electrolyte.

3.3. Proposed coating degradation mechanism

Building upon the aforementioned findings, the authors propose the following mechanism for the evolution of the coating pore resistance, as illustrated in Fig. 11. This process initiates with the exposure of the coating to the electrolyte. Within 24 h, the electrolyte fully permeates the coating, achieving complete saturation and causing the pore resistance to rapidly decline [36–39,52–54]. Simultaneously, the gradual dissolution of strontium chromate, a constituent of the coating, commences [55–57]. Although this dissolution generates pores or vacant spaces formerly occupied by strontium chromate, for coating #5903, #4215, #2547 and the newly applied coating, the pore resistance is observed to increase again after 48 h of immersion.

Concurrently with the leaching of strontium chromate, there appears to be a transport of aluminium through the coating. This aluminium might originate from the aluminium impurities present in the talc particles or from the bare aluminium substrate due to electrochemical reactions or from the anodized oxide layer, where Al_2O_3 can hydrolyse into aluminium (hydr)oxide gel upon interaction with water [58–61]. It is crucial to emphasize that no corrosion has been detected underneath the anodized layer at any location, and SEM examinations have not revealed any degradation of the anodized layer. This suggests that the scale at which aluminium dissolves may be beyond the resolution of the SEM. Nevertheless, it is established that aluminium undergoes dissolution, resulting in the formation of an aluminium (hydr)oxide gel at the surface of and likely within the coating's pores and transport pathways, thereby impeding ion mobility.

The authors suggest that the aluminium (hydr)oxide gel present in the coating undergoes chromate adsorption in the presence of chromate, forming Al^{3+}-O-Cr^{6+} bonds [62–64]. The adsorption of chromate onto aluminium (hydr)oxide-gel creates a dipolar structure that hinders electron transfer [64,65]. Consequently, this results in an increase in the pore resistance of the coating, as evidenced by EIS measurements, indicating that transport pathways are blocked. As illustrated in Fig. 11c, this blockage of transport pathways can occur particularly in/at: 1) the pores of the coating; 2) the pigment-particle epoxy-matrix interface of the coating; 3) the anodized oxide layer and/or 4) the interface between the metallic substrate and the coating-anodized oxide layer [57,66,67]. It is essential to consider that SEM analysis reveals the

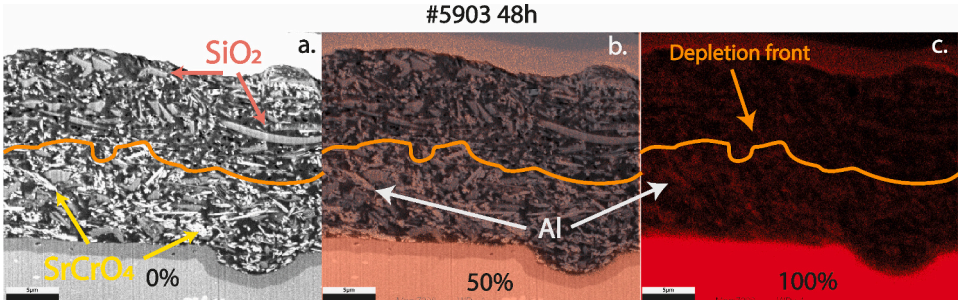

Fig. 9. SEM-BSE image of a cross section from coating #5903 following 48 h immersion in 0.1 M NaCl overlaying with a (a) 100 %, (b) 50 % or (c) 0 % transparent EDX image illustrating the distribution of aluminium within an epoxy coating.

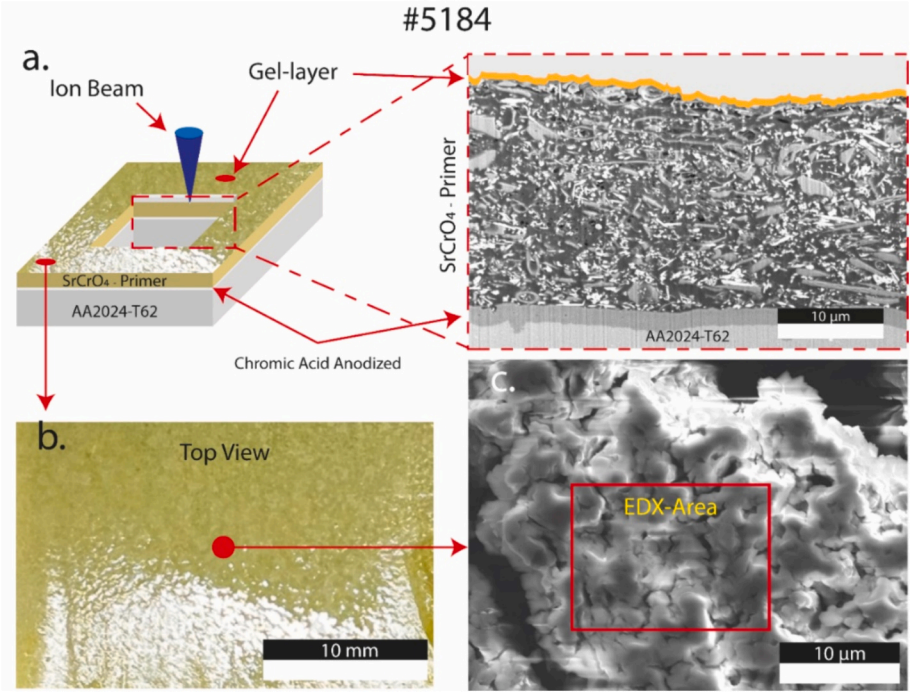

Fig. 10. Gel-like substance observed on top of coating #5184 after 1008 h of immersion testing. (a) Cross-sectional view of the coating obtained through FIB milling, with the location of the detected gel schematically highlighted in orange; (b) Top view of the coating, displaying the presence of the gel-layer; and (c) SEM image of the extracted (dried) gel-like substance, indicating the area where EDX analysis was conducted. (This gel layer was visually observed on top of coating #5184 and #2547. Since the gel layer was not observed on top of the other coatings, no further analysis was conducted for these samples.)

Table 2
EDX results revealing the composition of the gel-like substance situated on top of the coating, as illustrated in Fig. 10c.

Element, Line	Element Wt%	Wt% Error	Element At. %
C K	3,21	±0,02	5,37
O K	49,88	±0,26	62,67
Na K	4,62	±0,02	4,04
Al K	26,10	±0,09	19,45
Cl K	12,37	±0,04	7,01
Cr K	2,85	±0,02	1,10
Other	0,96	–	0,36

presence of large pores resulting from dissolved strontium chromate particles, without corresponding evidence of aluminium hydroxide products at these locations. This suggests that after prolonged immersion, it appears improbable that transport pathways associated with the pores in the organic coating are blocked. The authors consider it more plausible that the transport pathways along the pores of the anodized oxide layer were blocked instead; these could be sealed by the formation of aluminium (hydr)oxide while in contact with water [45,58]. Nevertheless, no supporting evidence exists for this claim, necessitating further investigations to elucidate this intricate interplay within the entire functional coating system.

3.4. Effect of degraded epoxy matrix on chromate leaching kinetics

3.4.1. Hypothesis for variations in leaching characteristics

The explanation provided for the increased pore resistance after 48 h of immersion, as shown in Fig. 6a, applies to coating #2547, #4215, #5903 and the newly applied coating. However, coating #5183 does not show a similar increase. Studying the change in capacitance alongside the pore resistance during immersion reveals a consistent pattern: the capacitance of coating #5183 remains almost unchanged, as shown in Fig. 6b. This effect is noticeable even after 48 h of immersion, an exposure duration at which significant changes occur in coatings #5903, #4215, #2547 and the newly applied coating.

SEM analysis in Fig. 7 indicates that coating #5183 shows a lower strontium chromate leaching, which could explain this phenomenon. To investigate the potential influence of the epoxy-polymer matrix on the leaching rate of strontium chromate, ATR-FTIR analyses were conducted. The hypothesis underlying these analyses is that differences in the polymer matrix may account for the observed variations in the leaching rate of strontium chromate [35,68].

3.4.2. ATR-FTIR measurements of aircraft coatings after service

The ATR-FTIR spectra for the measured coatings are depicted in Figs. 12 and 13, illustrating aircraft coatings after service as well as pristine coatings. In Fig. 12, a noticeable difference is observed, particularly in the case of #4215 as compared to the other coatings. This distinction is evident, especially in the peak bandwidths at 1010 cm^{-1} and 1085 cm^{-1} [69–73]. The peak at 1010 cm^{-1} suggests that coating #4215 has a higher concentration of C—O bonds than the other coatings, whereas the peak at 1085 cm^{-1} indicates a lower concentration of C—N bonds.

The higher concentration of C—O bonds in coating #4215 may imply the presence of a significant number of intact epoxy rings of DGEBA. Conversely, the lower concentration of C—N bonds suggests a limited presence of TETA bonds with the epoxy rings of DGEBA. This leads to the conclusion that during the application of coating #4215, likely an insufficient amount or the wrong type of hardener was added, resulting in a polymer with fewer cross-linked epoxy-polymer bonds. This reduced cross-linking could explain the rapid absorption of electrolyte and the subsequent faster leaching of strontium chromate. However, considering the data presented in Fig. 8, the leaching rate of the coating with the most flight hours, coating #5903, is even higher.

Due to the substantial deviation caused by the hardener, which influences the absorption properties of the epoxy matrix, coating #4215 is excluded from further analysis and discussion in comparison to the other spectra.

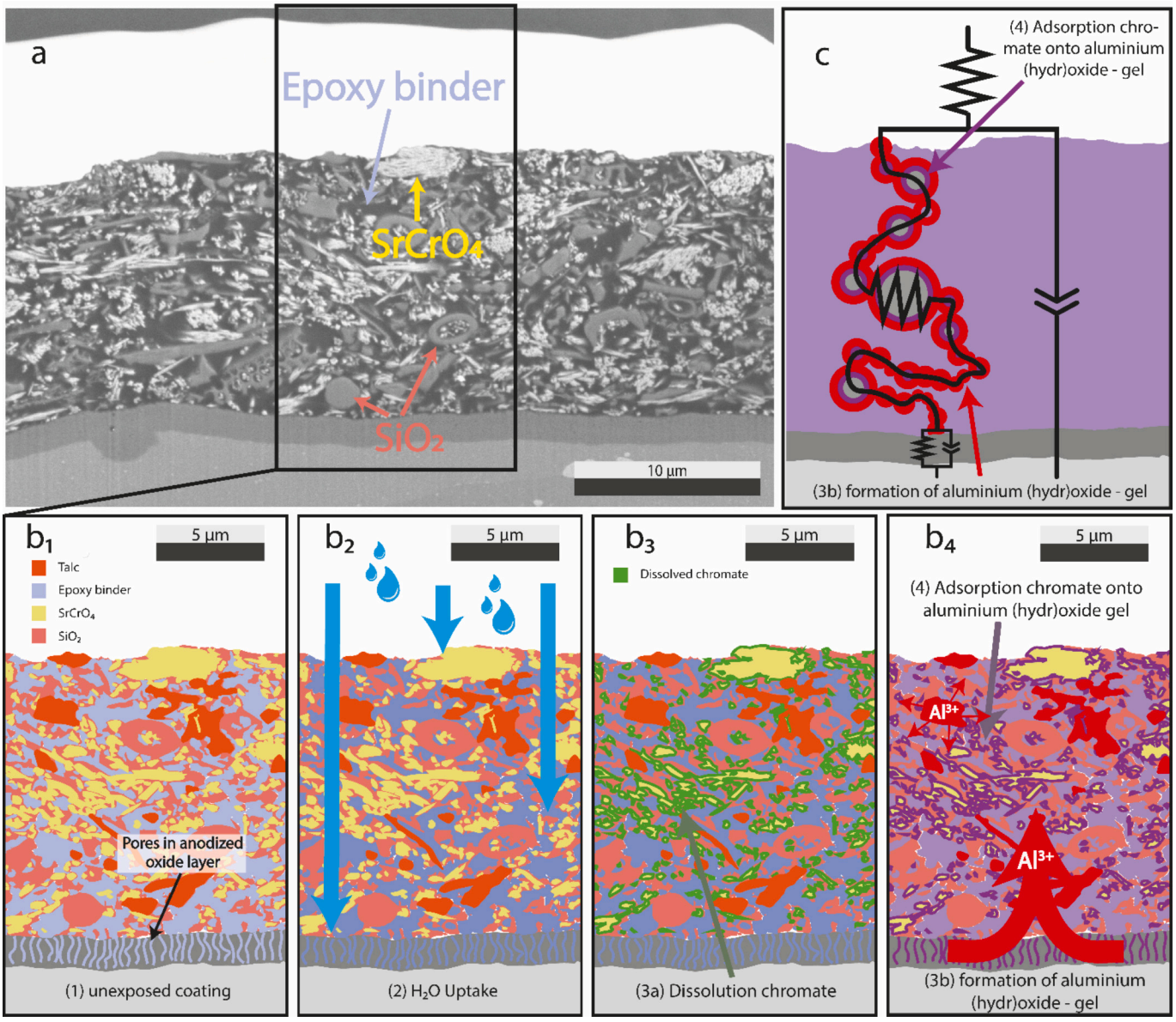

Fig. 11. Graphical representation of mechanisms influencing coating degradation during immersion in electrolyte. (a) SEM-BSE image indicating the region of interest, (b_1) unexposed coating, (b_2) water uptake in coating, (b_3) subsequent dissolution of strontium chromate, (b_4) dissolution of Al ions forming aluminium (hydr)oxide gel with the adsorption of chromate, (c) electrochemical representation corresponding to image (b_4).

In Fig. 12, variations in the adsorption at 1233 cm^{-1} are evident. The peak at 1233 cm^{-1} is indicative of an abundance of C-O-C-C bonds, highlighting a higher relative concentration of these bonds in the new coatings as compared to the coatings on the aircraft parts [73–75]. The difference in C-O-C-C bonds may be attributed to the extent of thermo-oxidation within each coating. Thermal exposure has the potential for breakdown of the C-O-C-C bonds in the crosslinked epoxy network, as illustrated in Fig. 14 [18,76–78]. Notably, this thermo-oxidation is most pronounced in coating #5903, followed by #2547. This observation implies that the epoxy matrix of #5183 remains nearly intact, resulting in a dense cross-linked polymer that hinders the easy transport of ions [41,79]. Consequently, the leaching of strontium chromate from the coating is less pronounced in coating #5183.

Another interesting result is the O—H adsorption at 3400 cm^{-1}, displaying variations among different coatings prior to immersion testing, as illustrated in Fig. 13 [73,80,81]. Although this adsorption may imply the presence of water inside the coating or the influence of a partially thermally oxidized coating, as demonstrated in Fig. 14, it could also be attributed to metal-hydroxide groups [18,47,77,78]. The differences in water concentrations among the different coatings can be ruled out, considering that all samples were stored together in a dry laboratory environment for several months before measuring IR spectra. This storage duration allowed the coatings to fully release potentially entrapped water inside, resulting in nearly identical and low water concentrations across all different coatings [82]. When contemplating the effects of thermo-oxidation on the O—H absorption peaks in the epoxy matrix, as illustrated in Fig. 14, it becomes apparent that the O—H absorption peak, as assigned in the coatings, is more appropriately associated with the bandwidth at 3400 cm^{-1} rather than the bandwidth at 3200–3300 cm^{-1}. According to literature, the bandwidth at 3200–3300 cm^{-1} is related to thermal oxidation, suggesting that other factors would influence the 3400 cm^{-1} bandwidths [18]. To further ascertain that the differences cannot be solely ascribed to thermo-oxidation, tests were conducted where newly coated samples were subjected to elevated temperatures for 7 days, as illustrated in Fig. 15. These tests reveal enhanced O—H absorption peaks at 3400 cm^{-1} when

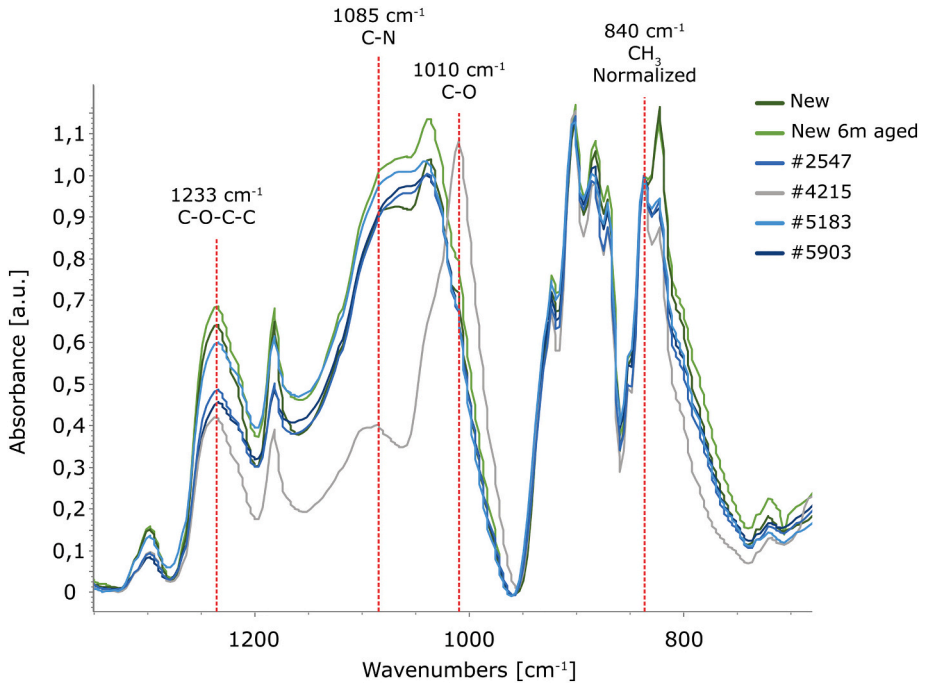

Fig. 12. ATR-FTIR spectra, spanning the range of 1350–650 cm^{-1}, depicting aircraft coatings after service as well as pristine coatings. All spectra are normalized at the peak at 840 cm^{-1}.

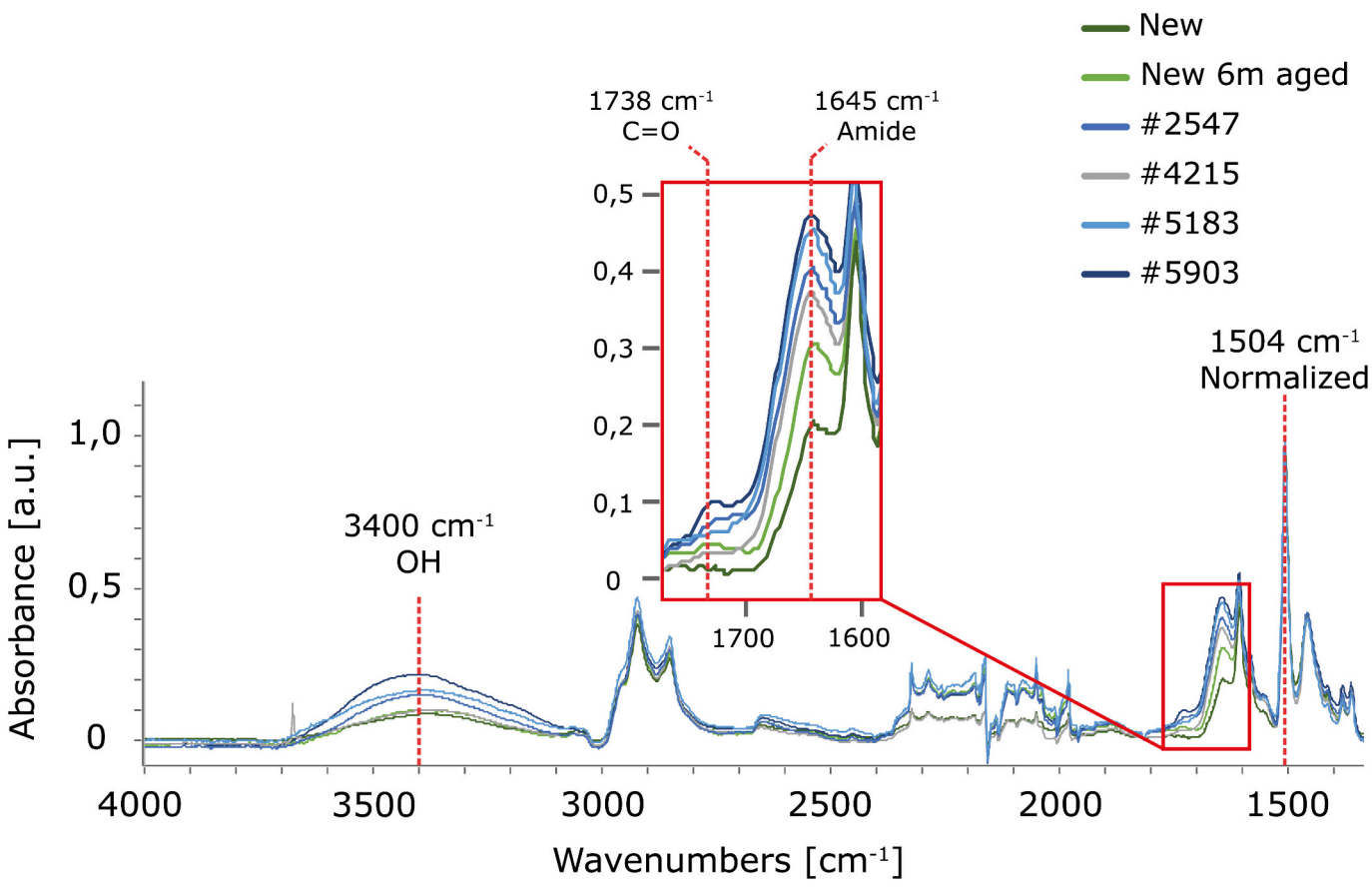

Fig. 13. ATR-FTIR spectra (4000–1325 cm^{-1}) comparing aged aircraft coatings after service with a pristine coating, highlighting the impact of thermo-oxidation at 1738 cm^{-1} & 1645 cm^{-1}, indicating the growth of hydroxide within the coating. Spectra are normalized at the peak at 1508 cm^{-1}.

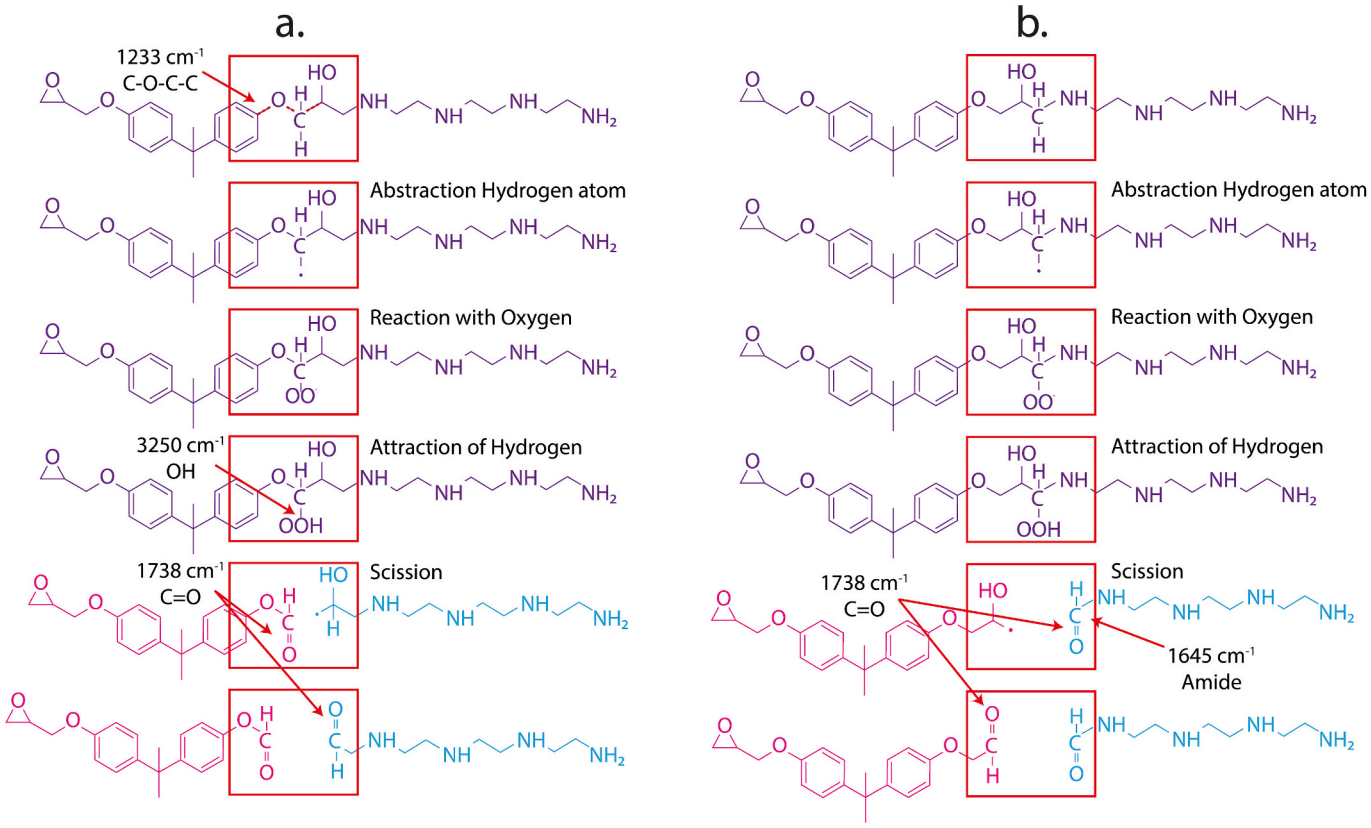

Fig. 14. Thermo-oxidation reaction at the DGEBA resin (a) and the TETA hardener (b), depicting the progression from an unaffected polymer chain to a fully oxidized chain, and elucidating the impact on the FTIR absorbance bandwidth.

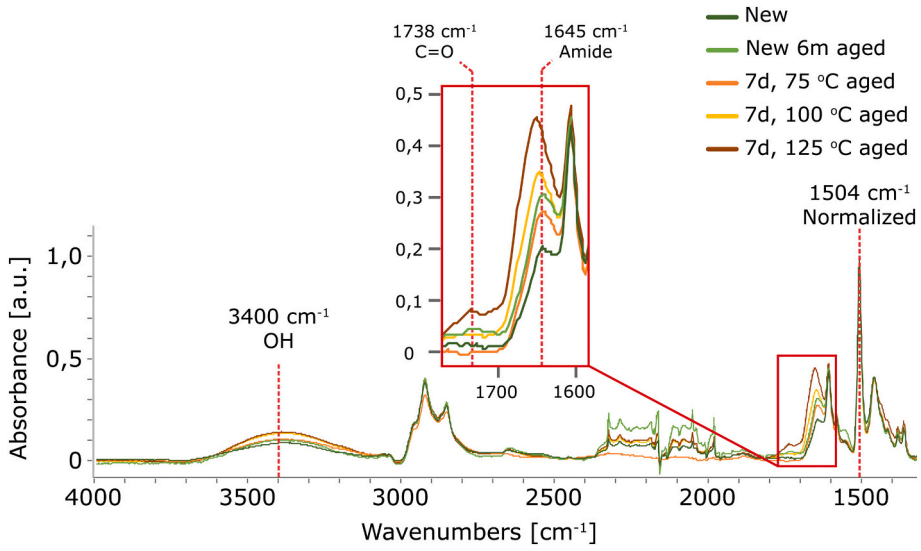

Fig. 15. ATR-FTIR spectra (4000–1325 cm^{-1}) comparing thermally-aged coatings with newly applied coatings, highlighting the impact of thermo-oxidation at 1738 cm^{-1} and 1645 cm^{-1} and showcasing the growth of hydroxide within the coating. Spectra are normalized at 1508 cm^{-1}.

thermo-oxidation is linked to the bandwidths at 1738 cm^{-1} and 1645 cm^{-1}. However, the intensity observed is significantly lower as compared to that experienced in aircraft parts before immersion testing, as presented in Fig. 13. This indicates that the ascribed O—H absorption peak represents the presence of metal-hydroxide bonds as well. Furthermore, this finding aligns with earlier results, as exemplified in Figs. 9 and 10, where the presence of aluminium inside and on top of the organic coatings was identified during immersion testing.

As a consequence, it can be assumed that before subjecting the coatings to an immersion test, varying concentrations of probably aluminium (hydr)oxide are already present inside the different coatings, as revealed by the ATR-FTIR analysis. The highest concentration was observed inside coating #5903, which has accumulated the highest number of flight hours, followed by #5183 and #2547, which were closely aligned, as shown in Fig. 13. While this trend offers only limited insights, it still suggests that #5903 has likely encountered the largest

exposure to electrolyte during operational service.

The assumption that the formation of hydroxides within the coatings implies the presence of internal pores or cracks is challenged by SEM analysis, which indicates an absence of such imperfections at the microscale, along with virtually no leachable strontium chromate. The degradation process in the coatings likely occurred exclusively at the nanoscale, with minimal exposure to electrolytes; otherwise, strontium chromate would have dissolved at the microscale [83]. Given the low solubility of strontium chromate, it can be assumed that these coatings have only experienced low levels of electrolyte exposure. This exposure could potentially result from a day/night cycle or a flight cycle, wherein a cold structure, upon contact with warmer air during landing or at the beginning of the day, induces condensation on the coated structure [84,85]. These minimal amounts of electrolyte may have contributed to the formation of aluminium (hydr)oxides inside the coating.

Thermo-oxidation is further supported by the observed peaks at the bandwidths of 1738 cm^{-1} and 1645 cm^{-1}, indicative of the presence of C═O bonds and amide groups, as depicted in Fig. 14b [18,73,76–78]. The peaks identified at the bandwidths of 1233 cm^{-1} and 1645 cm^{-1} suggest that oxidation predominantly transpires at the terminal NH_2 groups of the TETA hardener, which have undergone polymerization with the DGEBA epoxy [18,74–77]. However, it is important to note that the peak at a bandwidth of 1738 cm^{-1} is relatively weak, which complicates the formulation of any conclusions. The peak only remains clear for coating #5903, indicating that the largest amount of thermo-oxidation had taken place inside this coating.

A closer examination of the 1645 cm^{-1} bandwidth might suggest that thermo-oxidation has occurred inside the new coating after 6 months of aging. However, this is not supported when considering the 1233 cm^{-1} bandwidth. This distorted perspective may arise from the challenges encountered in normalizing FT-IR spectra of different pigmented coatings, as observed in this study, probably due to inevitable variations in pigment/epoxy matrix ratios.

3.4.3. Thermo-oxidation test

In order to scrutinize the ramifications of thermo-oxidation, a selection of tests was undertaken. Firstly, the influence of sunlight on the temperature variation of aircraft components was explored, of which the outcomes are delineated in Fig. 16. It is notable that the surface temperature of the matte-coated test samples markedly deviates from both the ambient temperature and the temperature within the box, where the ambient temperature closely aligns with the box temperature. The surface temperatures of the test panels can reach values up to 80 °C, when the ambient temperature hovers around 30 °C. This underscores that, in several regions around the globe, the aircraft skin temperatures can readily surpass 80 °C. Consequently, it is conceivable that coatings undergo degradation due to thermo-oxidation under operational conditions.

In order to gain deeper insights into the degradation induced by thermo-oxidation in coatings, reconstructed samples underwent a 7-day exposure to various temperatures. Subsequent to this exposure, ATR-FTIR measurements were performed. The findings are illustrated in Figs. 15 and 17. Much like the aircraft coating, an initial decline in C-O-C-C bonds is evident, as depicted in Fig. 17, particularly in the peak at 1233 cm^{-1} [73–75]. This decline correlates with the coating temperature during the aging process. Notably, no significant difference is noted between unheated coatings and those exposed to 75 °C for a duration of 7 days. However, the decline does become discernible when the coating experiences temperatures of 100 °C or higher.

A parallel trend is observed in Fig. 15 concerning amide formation at the 1645 cm^{-1} peak [18,73,76–78]. The formation of amide is not identified in new coatings and in coatings aged at 75 °C, potentially due to insufficient oxidation duration. Furthermore, the peak formation at 3400 cm^{-1}, indicative of OH formation, supports the assertion that 7 days at 75 °C does not lead to thermo-oxidation. However, literature indicates that coatings subjected to lower temperatures, such as 75 °C, for an extended time exhibit pronounced thermo-oxidation in a DGEBA-TETA epoxy [18,76]. This supports the notion that thermo-oxidation during the service life of coatings is a degradation factor that warrants consideration.

3.4.4. Graphical representation of coating degradation

Based on the findings elucidated in this study, a graphical representation of coating degradation is depicted in Fig. 18. It is posited that thermo-oxidation phenomena within a coating (Fig. 18b), particularly under moist conditions, may intensify the ingress of electrolytes into the coating matrix, as illustrated in Fig. 18c. This enhanced absorption is postulated to occur, at least in part, through the nanopores generated by the scission effect inherent in thermo-oxidation processes. The increased moisture absorption may facilitate a more rapid leaching of inhibitors from the coatings as depicted in Fig. 18d, enhancing their immediate efficacy in actively countering corrosion. However, within the intact coating region, the consequential formation of substantial pores compromises the coating barrier properties, thereby diminishing its capacity to furnish sustained protection against corrosion. It is hypothesized that these larger pores, coupled with nano defects in the epoxy matrix, reach an extent beyond repair through the subsequent formation of aluminium hydroxide and chromate adsorption, as illustrated in Fig. 18e.

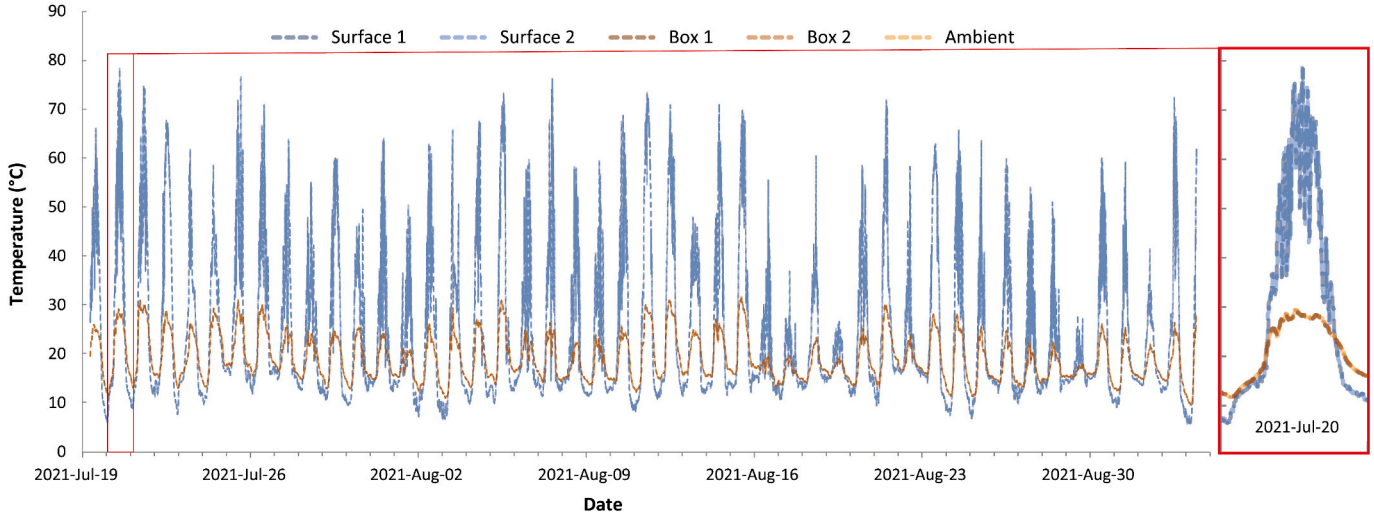

Fig. 16. Temperature evolution of the matte-coated surface in relation to ambient temperature and the temperature inside the box.

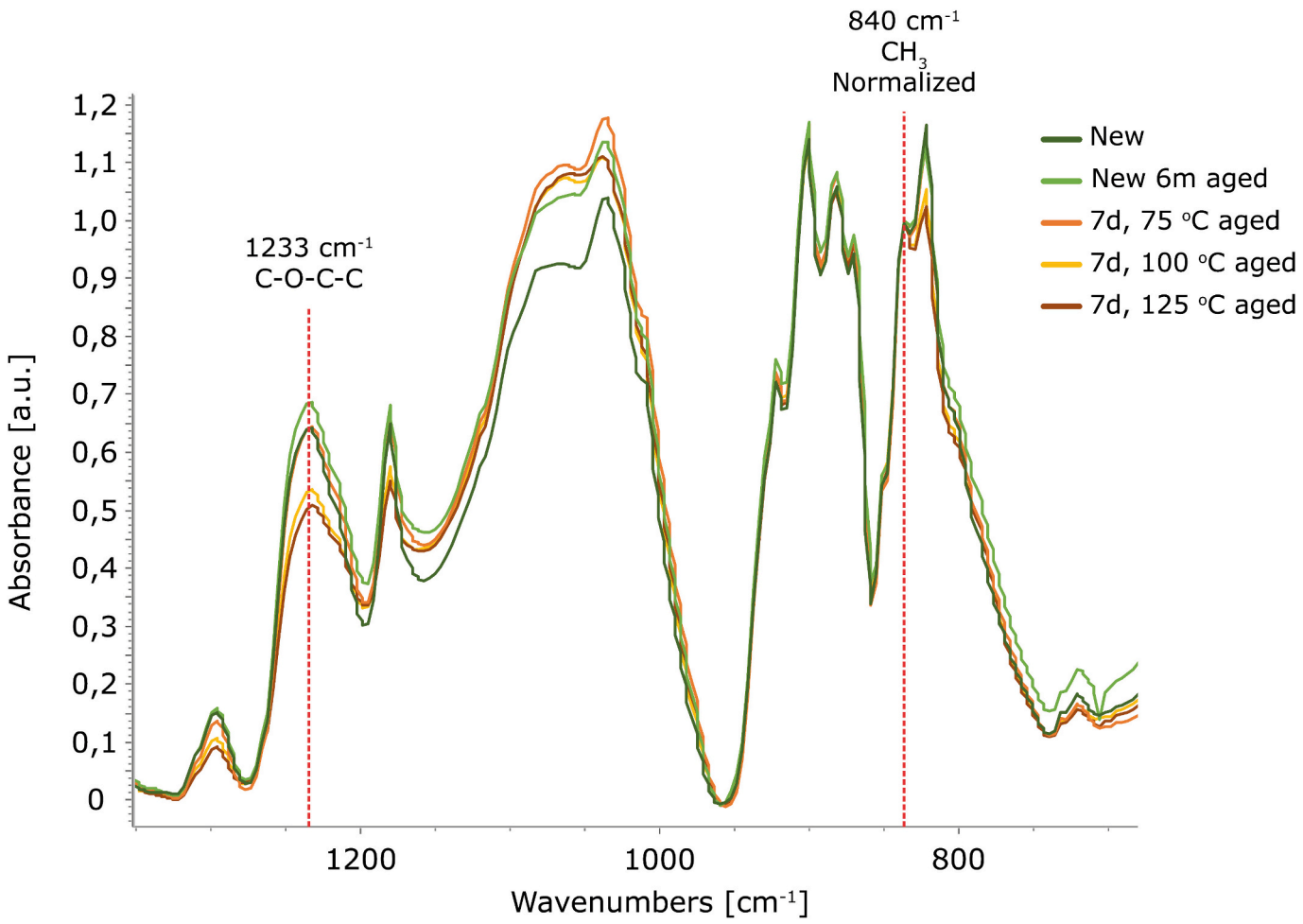

Fig. 17. ATR-FTIR spectra, covering the range of 1350–650 cm^{-1}, showcasing thermally aged coatings in comparison to newly applied coatings. All spectra are normalized at the peak at 840 cm^{-1}.

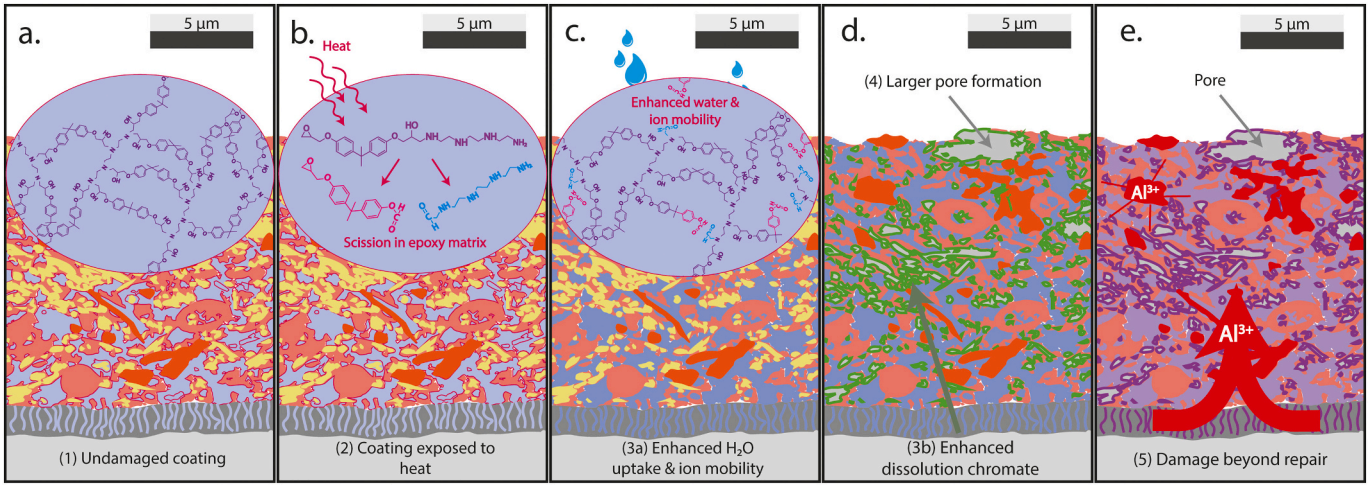

Fig. 18. The impact of thermal exposure on coating degradation: (a) intact epoxy matrix; (b) scission during exposure; (c) resulting enhanced ion mobility and water uptake; (d) accelerated dissolution of strontium chromate; (e) consequent formation of larger pores, irreparable by the formation of aluminium (hydr)oxides.

4. Conclusions

This study has underscored the paramount role of thermo-oxidation as a pivotal degradation factor in aged aircraft coatings. The study revealed that operational temperatures exceeding 80 °C, which trigger thermo-oxidation, result in accelerated electrolyte absorption and subsequent leaching of active inhibitors upon exposure to electrolyte. This cascade of events compromises the enduring corrosion protection offered by coatings, compelling the acknowledgment that thermo-oxidation is a degradation factor not to be underestimated when

coatings are exposed to substantial amounts of electrolyte.

An additional critical revelation pertains to the self-healing mechanism embedded within coatings, augmenting pore resistance during electrolyte exposure, an effect prominently demonstrated in the case of the coating with 5183 flight hours. This self-healing action is attributed to the dynamic mobility of aluminium emanating from the substrate, initiated after electrolyte absorption into the coating. These aluminium ions culminate in the formation of an aluminium hydroxide gel within the coating pores, onto which chromate from the coating adsorbs. This resulting product forms an efficacious barrier, amplifying coating resistance.

Furthermore, this study illuminates the consequential impact of application errors, exemplified by insufficient hardener addition to the paint, on coating performance. This underscores the indispensability of versatile technologies integrated into coatings, such as self-healing processes orchestrated by active inhibitors or metal hydroxide gel formation in the pores. These incorporated technologies in chromate-containing coating systems provide long-term protection even in instances of suboptimal application. The imperative now lies in incorporating these technologies into chromate-replacement coating systems, ensuring comparable or even improved corrosion protection for the intricate structures of aircraft.

Finally, the combination of EIS testing, EEC analysis and SEM analysis elucidates that the notable alterations in capacitance detected in coatings, as observed in EIS measurements, primarily stem from the leaching of inhibitors from the coating. This underscores the effectiveness of integrating EIS measurements with SEM analysis as a robust approach for investigating coating degradation.

CRediT authorship contribution statement

A.J. Cornet: Visualization, Methodology, Investigation, Formal analysis, Data curation, Conceptualization, Writing – original draft. **A. M. Homborg:** Supervision, Writing – review & editing. **L. 't Hoen-Velterop:** Supervision, Data curation, Writing – review & editing. **J.M. C. Mol:** Supervision, Writing – review & editing.

Declaration of competing interest

The authors declare that they have no known competing financial interests or personal relationships that could have appeared to influence the work reported in this paper.

Data availability

Data will be made available on request.

References

[1] L.N. Sukiman, X. Zhou, N. Birbilis, A.E. Hughes, J.M.C. Mol, S.J. Garcia, X. Zhou, E. G. Thompson, Durability and corrosion of aluminium and its alloys: overview, property space, techniques and developments, in: Aluminium Alloys - New Trends in Fabrication and Applications, InTech (2012), https://doi.org/10.5772/53752.

[2] A.E. Hughes, N. Birbilis, J.M.C. Mol, S.J. Garcia, Z. Xiaorong, G.E. Thompson, High strength Al-alloys: microstructure, corrosion and principles of protection, Recent Trends in Processing and Degradation of Aluminium Alloys (2011), https://doi.org/10.5772/18766.

[3] T. Mills, S. Prost-Domasky, K. Honeycutt, C. Brooks, Corrosion and the threat to aircraft structural integrity, Corrosion Control in the Aerospace Industry (2009) 35–66, https://doi.org/10.1533/9781845695538.1.35.

[4] J.V. Koleske, C.R. Hegedus, S.J. Spadafora, A.T. Eng, D.F. Pulley, D.J. Hirst, Aerospace and Aircraft Coatings, Paint and Coating Testing Manual 15th. Edition of the Gardner-Sward Handbook, 12, 2012, p. 739, https://doi.org/10.1520/mnl12239m.

[5] A. Jaya, U.H. Tiong, G. Clark, The interaction between corrosion management and structural integrity of aging aircraft, Fatigue Fract. Eng. Mater. Struct. (2012), https://doi.org/10.1111/j.1460-2695.2011.01562.x.

[6] A.E. Hughes, J.M.C. Mol, M.L. Zheludkevich, R.G. Buchheit, Active protective coatings (2016), https://doi.org/10.1007/978-94-017-7540-3_4.

[7] O. Gharbi, S. Thomas, C. Smith, N. Birbilis, Chromate replacement: what does the future hold? npj Mater. Degrad. 2 (2018) 23–25, https://doi.org/10.1038/s41529-018-0034-5.

[8] A.L. Holmes, S.S. Wise, J.P. Wise, Carcinogenicity of hexavalent chromium, Indian J. Med. Res. 128 (2008) 353–372.

[9] G. Bierwagen, D. Battocchi, A. Simões, A. Stamness, D. Tallman, The use of multiple electrochemical techniques to characterize mg-rich primers for Al alloys, Prog. Org. Coat. 59 (2007) 172–178, https://doi.org/10.1016/j.porgcoat.2007.01.022.

[10] P. Visser, Y. Liu, H. Terryn, J.M.C. Mol, Lithium salts as leachable corrosion inhibitors and potential replacement for hexavalent chromium in organic coatings for the protection of aluminum alloys, J. Coat. Technol. Res. 13 (2016) 557–566, https://doi.org/10.1007/s11998-016-9784-6.

[11] Z. Li, P. Visser, A.E. Hughes, A. Homborg, Y. Gonzalez-Garcia, A. Mol, Review of the state of art of Li-based inhibitors and coating technology for the corrosion protection of aluminium alloys, Surf. Coat. Technol. 478 (2024) 130441, https://doi.org/10.1016/J.SURFCOAT.2024.130441.

[12] G.S. Frankel, R.G. Buchheit, M. Jaworowski, G. Swain, Scientific Understanding of Non-Chromated Corrosion Inhibitors Function SERDP Project WP-1620, 2013.

[13] O.P. Ostash, I.M. Andreiko, Y.V. Holovatyuk, Degradation of materials and fatigue durability of aircraft constructions after long-term operation, Mater. Sci. 42 (2006), https://doi.org/10.1007/s11003-006-0098-1.

[14] J. Dante, Accelerated Dynamic Corrosion Test Method Development, 2017.

[15] L.M. Klyatis, Trends in development of accelerated testing for automotive and aerospace, engineering (2020), https://doi.org/10.1016/B978-0-12-818841-5.01001-1.

[16] R.J. Varley, E.K. Simmonds, J.E. Seebergh, D.H. Berry, Investigation of factors impacting the in-service degradation of aerospace coatings, Prog. Org. Coat. (2012), https://doi.org/10.1016/j.porgcoat.2011.09.026.

[17] A.J. Cornet, A.M. Homborg, P.R. Anusuyadevi, L. 't Hoen-Velterop, J.M.C. Mol, Unravelling corrosion degradation of aged aircraft components protected by chromate-based coatings, Eng. Fail. Anal. 159 (2024) 108070, https://doi.org/10.1016/j.engfailanal.2024.108070.

[18] S. Morsch, Y. Liu, S.B. Lyon, S.R. Gibbon, B. Gabriele, M. Malanin, K.J. Eichhorn, Examining the early stages of thermal oxidative degradation in epoxy-amine resins, Polym. Degrad. Stab. 176 (2020) 109147, https://doi.org/10.1016/j.polymdegradstab. 2020.109147.

[19] J. Fang, L. Zhang, D. Sutton, X. Wang, T. Lin, Needleless melt-electrospinning of polypropylene nanofibres, J. Nanomater. 2012 (2012), https://doi.org/10.1155/2012/382639.

[20] B. Wouters, E. Jalilian, R. Claessens, N. Madelat, T. Hauffman, G. Van Assche, H. Terryn, A. Hubin, Monitoring initial contact of UV-cured organic coatings with aqueous solutions using odd random phase multisine electrochemical impedance spectroscopy, Corros. Sci. 190 (2021) 109713, https://doi.org/10.1016/j.corsci.2021.109713.

[21] T. Bos, Prediction of Coating Durability - Early Detection Using Electrochemical Methods, 2008.

[22] A. Xu, F. Zhang, F. Jin, R. Zhang, B. Luo, T. Zhang, The evaluation of coating performance by analyzing the intersection of bode plots, Int. J. Electrochem. Sci. 9 (2014) 5116–5125, https://doi.org/10.1016/S1452-3981(23)08155-5.

[23] Y. Zuo, R. Pang, W. Li, J.P. Xiong, Y.M. Tang, The evaluation of coating performance by the variations of phase angles in middle and high frequency domains of EIS, Corros. Sci. 50 (2008) 3322–3328, https://doi.org/10.1016/j.corsci.2008.08.049.

[24] P. Visser, M. Meeusen, Y. Gonzalez-Garcia, H. Terryn, J.M.C. Mol, Electrochemical evaluation of corrosion inhibiting layers formed in a defect from lithium-leaching organic coatings, J. Electrochem. Soc. 164 (2017), https://doi.org/10.1149/2.1411707jes.

[25] J.-M. Hu, J.-T. Zhang, J.-Q. Zhang, C.-N. Cao, A novel method for determination of diffusion coefficient of corrosive species in organic coatings by EIS, J. Mater. Sci. 39 (2004) 4475–4479, https://doi.org/10.1023/b:jmsc.0000034140.96862.1a.

[26] I.C.P. Margarit-Mattos, EIS and organic coatings performance: revisiting some key points, Electrochim. Acta 354 (2020) 136725, https://doi.org/10.1016/j.electacta.2020.136725.

[27] Q. Zhou, Y. Wang, Comparisons of clear coating degradation in NaCl solution and pure water, Prog. Org. Coat. 76 (2013) 1674–1682, https://doi.org/10.1016/j.porgcoat.2013.07.018.

[28] Z. Feng, G.S. Frankel, Evaluation of coated Al alloy using the breakpoint frequency method, Electrochim. Acta 187 (2016) 605–615, https://doi.org/10.1016/j.electacta.2015.11.114.

[29] E.B. Caldona, D.O. Wipf, D.W. Smith, Characterization of a tetrafunctional epoxy-amine coating for corrosion protection of mild steel, Prog. Org. Coat. 151 (2021), https://doi.org/10.1016/j.porgcoat.2020.106045.

[30] G. Liu, Y. Zhang, M. Wu, R. Huang, Study of depassivation of carbon steel in simulated concrete pore solution using different equivalent circuits, Constr. Build. Mater. 157 (2017), https://doi.org/10.1016/j.conbuildmat.2017.09.104.

[31] B.Y. Chang, Conversion of a constant phase element to an equivalent capacitor, J. Electrochem. Sci. Technol. 11 (2020) 318–321, https://doi.org/10.33961/jecst.2020.00815.

[32] J.M. Vega, N. Granizo, D. De La Fuente, J. Simancas, M. Morcillo, Corrosion inhibition of aluminum by coatings formulated with Al-Zn-vanadate hydrotalcite, Prog. Org. Coat. 70 (2011), https://doi.org/10.1016/j.porgcoat.2010.08.014.

[33] Y. Zhu, J. Xiong, Y. Tang, Y. Zuo, EIS study on failure process of two polyurethane composite coatings, Prog. Org. Coat. 69 (2010), https://doi.org/10.1016/j.porgcoat.2010.04.017.

[34] V. Lavaert, M. De Cock, M. Moors, E. Wettinck, Influence of pores on the quality of a silicon polyester coated galvanized steel system, Prog. Org. Coat. 38 (2000), https://doi.org/10.1016/S0300-9440(00)00107-7.

[35] V. Wachtendorf, U. Kalbe, O. Krüger, N. Bandow, Influence of weathering on the leaching behaviour of zinc and PAH from synthetic sports surfaces, Polym. Test. 63 (2017), https://doi.org/10.1016/j.polymertesting.2017.09.021.

[36] M. Hoseinpoor, T. Prošek, L. Babusiaux, J. Mallégol, Simplified approach to assess water uptake in protective organic coatings by parallel plate capacitor method, Mater. Today Commun. 26 (2021), https://doi.org/10.1016/j.mtcomm.2020.101858.

[37] A.S. Nguyen, N. Causse, M. Musiani, M.E. Orazem, N. Pébère, B. Tribollet, V. Vivier, Determination of water uptake in organic coatings deposited on 2024 aluminium alloy: comparison between impedance measurements and gravimetry, Prog. Org. Coat. 112 (2017), https://doi.org/10.1016/j.porgcoat.2017.07.004.

[38] E.P.M. van Westing, G.M. Ferrari, J.H.W. de Wit, The determination of coating performance with impedance measurements-II. Water uptake of coatings, Corros. Sci. 36 (1994), https://doi.org/10.1016/0010-938X(94)90197-X.

[39] E.P.M. van Westing, G.M. Ferrari, J.H.W. De Wit, The determination of coating performance using electrochemical impedance spectroscopy, Electrochim. Acta 39 (1994) 899–910, https://doi.org/10.1016/0013-4686(94)85104-2.

[40] A. Vedadi, X. Wang, M.S. Parvej, Q. Yuan, F. Azarmi, D. Battocchi, Z. Lin, Y. Wang, Degradation of epoxy coatings exposed to impingement flow, J. Coat. Technol. Res. 18 (2021) 1153–1164, https://doi.org/10.1007/s11998-021-00472-2.

[41] F. Deflorian, S. Rossi, An EIS study of ion diffusion through organic coatings, Electrochim. Acta 51 (2006) 1736–1744, https://doi.org/10.1016/j.electacta.2005.02.145.

[42] J.M. Vega, N. Granizo, J. Simancas, D. De La Fuente, I. Díaz, M. Morcillo, Corrosion inhibition of aluminum by organic coatings formulated with calcium exchange silica pigment, J. Coat. Technol. Res. 10 (2013), https://doi.org/10.1007/s11998-012-9440-8.

[43] Z. (Vivian) Ding, B.A. Smith, R.R. Hebert, W. Zhang, M.R. Jaworowski, Morphology perspective on chromic acid anodizing replacement by thin film sulfuric acid anodizing, Surf. Coat. Technol. 350 (2018), https://doi.org/10.1016/j.surfcoat.2018.07.008.

[44] A. Carangelo, M. Curioni, A. Acquesta, T. Monetta, F. Bellucci, Application of EIS to in situ characterization of hydrothermal sealing of anodized aluminum alloys: comparison between hexavalent chromium-based sealing, hot water sealing and cerium-based sealing, J. Electrochem. Soc. 163 (2016), https://doi.org/10.1149/2.0231610jes.

[45] N. Hu, X. Dong, X. He, J.F. Browning, D.W. Schaefer, Effect of sealing on the morphology of anodized aluminum oxide, Corros. Sci. 97 (2015), https://doi.org/10.1016/j.corsci.2015.03.021.

[46] G. Grundmeier, W. Schmidt, M. Stratmann, Corrosion protection by organic coatings: electrochemical mechanism and novel methods of investigation, Electrochim. Acta 45 (2000), https://doi.org/10.1016/S0013-4686(00)00348-0.

[47] Y. Dong, Q. Zhou, Relationship between ion transport and the failure behavior of epoxy resin coatings, Corros. Sci. 78 (2014) 22–28, https://doi.org/10.1016/j.corsci.2013.08.017.

[48] R. Thomas, D. Grose, G. Obaje, R. Taylor, N. Rowson, S. Blackburn, Residence time investigation of a multiple hearth kiln using mineral tracers, Chem. Eng. Process. Process Intensif. 48 (2009), https://doi.org/10.1016/j.cep.2009.01.003.

[49] J.B. Jurinski, J.D. Rimstidt, Biodurability of talc, Am. Mineral. 86 (2001), https://doi.org/10.2138/am-2001-0402.

[50] P.S. Rao, B.J. Reddy, Spectroscopic investigations on different grade samples of talc, Radiat. Eff. Defects Solids 127 (1993), https://doi.org/10.1080/10420159308220312.

[51] V. Atluri, J. Jin, K. Shrimali, L. Dang, X. Wang, J.D. Miller, The hydrophobic surface state of talc as influenced by aluminum substitution in the tetrahedral layer, J. Colloid Interface Sci. 536 (2019), https://doi.org/10.1016/j.jcis.2018.10.085.

[52] Z. Manoli, D. Pecko, G. Van Assche, J. Stiens, A. Pourkazemi, H. Terryn, Transport of Electrolyte in Organic Coatings on Metal, in: Paint and Coatings Industry, IntechOpen, 2019, https://doi.org/10.5772/intechopen.81422.

[53] G.K. Van Der Wel, O.C.G. Adan, Moisture in organic coatings - a review, Prog. Org. Coat. 37 (1999) 1–14, https://doi.org/10.1016/S0300-9440(99)00058-2.

[54] S. Morsch, S. Emad, S.B. Lyon, S.R. Gibbon, M. Irwin, The location of adsorbed water in pigmented epoxy-amine coatings, Prog. Org. Coat. 173 (2022) 107223, https://doi.org/10.1016/j.porgcoat.2022.107223.

[55] T. Prosek, D. Thierry, A model for the release of chromate from organic coatings, Prog. Org. Coat. 49 (2004) 209–217, https://doi.org/10.1016/j.porgcoat.2003.09.012.

[56] F.H. Scholes, S.A. Furman, A.E. Hughes, T. Nikpour, N. Wright, P.R. Curtis, C. M. Macrae, S. Intem, A.J. Hill, Chromate leaching from inhibited primers, Part I. Characterisation of leaching, Prog. Org. Coat. 56 (2006) 23–32, https://doi.org/10.1016/j.porgcoat.2006.01.015.

[57] S. Sellaiyan, A.E. Hughes, S.V. Smith, A. Uedono, J. Sullivan, S. Buckman, Leaching properties of chromate-containing epoxy films using radiotracers, PALS and SEM, Prog. Org. Coat. 77 (2014), https://doi.org/10.1016/j.porgcoat.2013.09.014.

[58] M.J. Bartolomé, V. López, E. Escudero, G. Caruana, J.A. González, Changes in the specific surface area of porous aluminium oxide films during sealing, Surf. Coat. Technol. 200 (2006), https://doi.org/10.1016/j.surfcoat.2005.03.019.

[59] B.C. Bunker, G.C. Nelson, K.R. Zavadil, J.C. Barbour, F.D. Wall, J.P. Sullivan, C. F. Windisch, M.H. Engelhardt, D.R. Baer, Hydration of passive oxide films on aluminum, J. Phys. Chem. B 106 (2002), https://doi.org/10.1021/jp013246e.

[60] C.A. Melendres, S. Van Gils, H. Terryn, Toward a quantitative description of the anodic oxide films on aluminum, Electrochem. Commun. 3 (2001), https://doi.org/10.1016/S1388-2481(01)00250-8.

[61] Hydrolysis of Metal Ions, 2016, https://doi.org/10.1002/9783527656189.

[62] B.M. Weckhuysen, I.E. Wachs, R.A. Schoonheydt, Surface chemistry and spectroscopy of chromium in inorganic oxides, Chem. Rev. 96 (1996) 3327–3349, https://doi.org/10.1021/cr940044o.

[63] J.D. Ramsey, R.L. McCreery, In situ Raman microscopy of chromate effects on corrosion pits in aluminum alloy, J. Electrochem. Soc. 146 (1999) 4076–4081, https://doi.org/10.1149/1.1392594.

[64] L. Xia, R.L. McCreery, Chemistry of a chromate conversion coating on aluminum alloy AA2024-T3 probed by vibrational spectroscopy, J. Electrochem. Soc. 145 (1998) 3083–3089, https://doi.org/10.1149/1.1838768.

[65] G.S. Frankel, C.R. Clayton, R.D. Granata, M. Kendig, H.S. Isaacs, R.L. McCreery, M. Stratmann, Mechanism of Al alloy corrosion and the role of chromate inhibitors (2001) 1–83.

[66] M. Kopeć, B.D. Rossenaar, K. van Leerdam, A.N. Davies, S.B. Lyon, P. Visser, S. R. Gibbon, Chromate ion transport in epoxy films: influence of BaSO4 particles, Prog. Org. Coat. 147 (2020), https://doi.org/10.1016/j.porgcoat.2020.105739.

[67] A.E. Hughes, A. Trinchi, F.F. Chen, Y.S. Yang, I.S. Cole, S. Sellaiyan, J. Carr, P. D. Lee, G.E. Thompson, T.Q. Xiao, The application of multiscale quasi 4D CT to the study of SrCrO4 distributions and the development of porous networks in epoxy-based primer coatings, Prog. Org. Coat. 77 (2014), https://doi.org/10.1016/j.porgcoat.2014.07.001.

[68] Y. Elkebir, S. Mallarino, D. Trinh, S. Touzain, Effect of physical ageing onto the water uptake in epoxy coatings, Electrochim. Acta 337 (2020), https://doi.org/10.1016/j.electacta.2020.135766.

[69] M. Tarnacka, M. Dulski, S. Starzonek, K. Adrjanowicz, E.U. Mapesa, K. Kaminski, M. Paluch, Following kinetics and dynamics of DGEBA-aniline polymerization in nanoporous native alumina oxide membranes - FTIR and dielectric studies, Polymer (Guildf) 68 (2015) 253–261, https://doi.org/10.1016/j.polymer.2015.05.022.

[70] G. Yang, X. Huang, J. Cai, Q. Zhang, Curing mechanism of triglycidylamine crosslinked soybean protein adhesive analyzed by Fourier transform infrared, second derivative infrared and two-dimensional correlation spectroscopy, Int. J. Adhes. Adhes. 107 (2021) 102825, https://doi.org/10.1016/j.ijadhadh.2021.102825.

[71] A. Patel, A. Maiorana, L. Yue, R.A. Gross, I. Manas-Zloczower, Curing kinetics of biobased epoxies for tailored applications, Macromolecules 49 (2016) 5315–5324, https://doi.org/10.1021/acs.macromol.6b01261.

[72] S. Farishi, A. Rifathin, B.F. Ramadhoni, Phosphorus/nitrogen grafted lignin as a biobased flame retardant for unsaturated polyester resin, Springer Singapore (2020), https://doi.org/10.1007/978-981-15-0950-6_65.

[73] G. Socrates, Infrared and Raman Characteristic Group Frequencies: Tables and Charts, 3rd edition, 2004.

[74] G.C. Bossier, Spectrometric Identification of Organic Compounds, 1962.

[75] R.A. Chowdhury, M.V. Hosur, M. Nuruddin, A. Tcherbi-Narteh, A. Kumar, V. Boddu, S. Jeelani, Self-healing epoxy composites: preparation, characterization and healing performance, J. Mater. Res. Technol. 4 (2015) 33–43, https://doi.org/10.1016/J.JMRT.2014.10.016.

[76] R. Delannoy, V. Tognetti, E. Richaud, Experimental and theoretical insights on the thermal oxidation of epoxy-amine networks, Polym. Degrad. Stab. 206 (2022) 110188, https://doi.org/10.1016/j.polymdegradstab. 2022.110188.

[77] A. Rivaton, L. Moreau, J.-L. Gardette, Photo-oxidation of phenoxy resins at long and short wavelengths—II, Mechanisms of formation of photoproducts, Polym. Degrad. Stab. 58 (1997) 333–339, https://doi.org/10.1016/S0141-3910(97)00088-8.

[78] A. Meiser, K. Willstrand, W. Possart, Influence of composition, humidity, and temperature on chemical aging in epoxies: a local study of the interphase with air, J. Adhes. 86 (2010) 222–243, https://doi.org/10.1080/00218460903418352.

[79] S.G. Croll, Electrolyte transport in polymer barrier coatings: perspectives from other disciplines, Prog. Org. Coat. 124 (2018) 41–48, https://doi.org/10.1016/j.porgcoat.2018.07.027.

[80] C. Ramírez, M. Rico, A. Torres, L. Barral, J. López, B. Montero, Epoxy/POSS organic – inorganic hybrids, ATR-FTIR and DSC studies 44 (2008) 3035–3045, https://doi.org/10.1016/j.eurpolymj.2008.07.024.

[81] P.R. Griffiths, The handbook of infrared and Raman characteristic frequencies of organic molecules, Vib. Spectrosc. 4 (1992), https://doi.org/10.1016/0924-2031(92)87021-7.

[82] J.H. Park, G.D. Lee, H. Ooshige, A. Nishikata, T. Tsuru, Monitoring of water uptake in organic coatings under cyclic wet-dry condition, Corros. Sci. 45 (2003), https://doi.org/10.1016/S0010-938X(03)00024-6.

[83] P. Iannarelli, D. Beaumont, Y. Liu, X. Zhou, T.L. Burnett, M. Curioni, S.B. Lyon, S. R. Gibbon, S. Morsh, S. Emad, T. Hashimoto, N. Hijnen, The degradation mechanism of a marine coating under service conditions of water ballast tank, Prog. Org. Coat. 162 (2022), https://doi.org/10.1016/j.porgcoat.2021.106588.

[84] J. Demo, F. Friedersdorf, Aircraft corrosion monitoring and data visualization techniques for condition based maintenance, IEEE Aerospace Conference Proceedings (2015), https://doi.org/10.1109/AERO.2015.7119048.

[85] J. Demo, F. Friedersdorf, Evaluation of environmental exposure and corrosive conditions within rotorcraft airframes, in: NACE - International Corrosion Conference Series, 2014.